Consortium for Small-Scale Modelling

Technical Report No. 44

The COSMO Priority Project CDIC: Comparison of the dynamical cores of ICON and COSMO, Final Report

October 2021

DOI: 10.5676/DWD_pub/nwv/cosmo-tr_44

Deutscher Wetterdienst
MeteoSwiss
Ufficio Generale Spazio Aereo e Meteorologia
ΕΘΝΙΚΗ ΜΕΤΕΩΡΟΛΟΓΙΚΗ ΥΠΗΡΕΣΙΑ
Instytut Meteorologii i Gospodarki Wodnej
Administratia Nationala de Meteorologie
ROSHYDROMET
Agenzia Regionale Protezione Ambiente Piemonte
Agenzia Regionale Prevenzione Ambiente Energia Emilia Romagna
Centro Italiano Ricerche Aerospaziali
Amt für GeoInformationswesen der Bundeswehr
Israel Meteorological Service

www.cosmo-model.org

Editor: Massimo Milelli, ARPA Piemonte

The COSMO Priority Project CDIC: Comparison of the dynamical cores of ICON and COSMO, Final Report

Michael Baldauf[1 *], *Damian Wojcik*[2], *Florian Prill*[1], *Daniel Reinert*[1], *Rodica Dumitrache*[3], *Amalia Iriza*[3], *Guy deMorsier*[4], *Marina Shatunova*[5], *Günther Zängl*[1], *Ulrich Schättler*[1]

[*] Project coordinator
[1] Deutscher Wetterdienst - DWD
[2] Instytut Meteorologii i Gospodarki Wodnej - IMGW
[3] Administratia Nationala de Meteorologie - NMA
[4] MeteoSwiss - MCH
[5] HydroMetCenter of Russia - RHM

Contents

1 Introduction

The ICON model development originally was a joint effort between the Deutscher Wetterdienst (DWD, Offenbach) and the Max-Planck Institute for Meteorology (MPI, Hamburg) with the aim to get a common modeling framework for global weather forecast and climate simulations. Later on, the Deutsches Klimarechenzentrum (DKRZ, Hamburg) and the Karlsruhe Institute for Technology (KIT, Karlsruhe) joined this model development. ICON became operational as a global model for NWP at DWD at 20 January 2015.

Although being a global model, ICON (Zängl et al., 2015) should be able to do simulations on the regional scale, too, first by two-way nesting (at 21 July 2015, the ICON-EU nest replaced the former COSMO-EU at DWD), and later on as an externally coupled limited-area model. In consequence, currently and in the following years the COSMO-Consortium (Consortium for Small-Scale Modelling) also joins the ICON-model development and the member states will replace the regional model COSMO (www.cosmo-model.org) (Doms and Baldauf, 2018; Baldauf et al., 2011) by the limited-area setup of ICON during the next years. The same holds for the COSMO licensee countries.

To support and to supervise this migration process and to maintain quality assurance at the several weather services for the replacement of a regional-scale NWP model, a few priority projects have been defined in the COSMO consortium. The goal of the priority project 'Comparison of the dynamical cores of ICON and COSMO' (PP CDIC) is an objective as possible assessment of the dynamical cores of both models. It was carried out mainly during the two year period 2016-2017. The need for such a comparison stems from the fact that it is not a priori clear if the triangle grid of ICON and some properties of its dynamical core (e.g. there is no time-splitting between slow and fast processes in the pure non-hydrostatic Euler equations), although being beneficial on the global scale, will be beneficial on the small (or regional) scale, too.

Section 2 gives a brief overview and comparison of the main properties of the dynamical cores of ICON and COSMO. Their assessment is mainly done by the evaluation of several (idealized) test cases that are typical for limited area models. Physical parameterizations are switched off as much as possible. These idealized test cases and their comparison of ICON and COSMO are discussed in section 3. Strong scaling properties on massively parallel computers are presented in section 4.

2 Brief overview and comparison of the dynamical core formulations of ICON and COSMO

In this section, a brief comparison between the dynamical cores of COSMO and ICON is given, more details can be found in Doms and Baldauf (2018) and Zängl et al. (2015), respectively. The dynamical cores of both models are based on the compressible, non-hydrostatic Euler equations (this holds for the new COSMO-EULAG development (Kurowski et al., 2016; Ziemiański et al., 2021), too. However, in the following only the operationally used so-called 'Runge-Kutta-version' of COSMO is considered). For operational setups, both models use the shallow atmosphere approximation (together with the traditional approximation for some Coriolis and spherical metric terms in the advection).

The prognostic variables of COSMO are pressure p', temperature T' (both perturbations from a reference state) and the 3 spherical velocity components u, v, w. ICON uses density ρ, either density weighted virtual potential temperature $\rho\Theta_v$ or Exner pressure Π (the latter for

easier vertically implicit time integration), vertical velocity w and the triangle edge normal component of the horizontal velocity v_n as prognostic variables (of course u and v can be diagnosed from v_n for each triangle and vice versa). To increase numerical accuracy, ICON again uses the deviations from a reference state of the thermodynamic variables (ρ', $(\rho\Theta_v)'$, or Π') in the dynamical core.

A basic difference between ICON and COSMO lies in the horizontal grid and the related discretizations. COSMO uses a structured (i.e. a rotated lat-lon) grid, whereas ICON uses a triangular grid based on successive subdivision of the triangles of an icosahedron. Horizontal discretizations use a staggered C-grid and vertically a Lorenz-grid: scalar variables (like ρ, T, p, ...) are positioned in the cell center; in the center of a cuboid in COSMO and in the center of a prism in ICON (more precise: this center is determined as the circumcentre of a triangle). In contrast, each edge normal velocity component sits in the center of the edge face. In spite of this formal similarity in the staggering, though one can apply simple finite-difference formulas in the case of COSMO, the discretizations in ICON merely must be constructed via the integral theorems of Gauss and Stokes. However, the application of the Gauss theorem in the continuity equation (i.e. a finite-volume approach) allows exact mass conservation in ICON. This is not possible in COSMO, since ρ is not a prognostic variable there.

In particular for the advection of these 'dynamic' variables, COSMO can use higher order schemes (although one-dimensional, direction-split) in the horizontal direction due to the simple finite-difference approach. In the convection-permitting setups, usually a fifth order scheme (Wicker and Skamarock, 2002) is used. In contrast, ICON has to use again second order discretizations. However, this is at least consistent to the other second order discretizations.

Concerning the time integration of the Euler equations, both dynamical cores use the horizontally explicit, vertically implicit (HEVI) approach. This treats the fast vertically expanding sound and gravity waves in an implicit manner, to avoid too small time steps. However, COSMO uses a split-explicit scheme to treat the remaining horizontal directions: the fast waves (sound and gravity waves) are integrated with a small time step, whereas the slower advection terms are treated with a larger time step. Both processes are combined by so-called partial operator splitting, which couples these processes better than complete operator splitting (Skamarock and Klemp, 1992) and to achieve at least second order in time a 3-stage Runge-Kutta scheme is used. This approach was first developed for the WRF model by Wicker and Skamarock (2002), and its stability properties for COSMO have been proven in Baldauf (2010). In contrast, ICON avoids the split-explicit method but integrates both the fast waves and the advection of the above mentioned dynamic variables with the same small time step (Zängl et al., 2015). The motivation stems from the fact that in a global model with higher model tops, the maximum advection velocities are not so far away from sound velocity, therefore, a split-explicit approach is obviously less advantageous for a global model than for a pure limited-area model like COSMO. To achieve second order in time a two-time-level predictor-corrector scheme is applied.

Apart from these fundamental discretization approaches, each dynamical core needs more or less additional measures for stabilization. For the vertically implicit integration both dynamical cores use some off-centering in the coefficients weighting the previous and the actual time level. In COSMO, quasi-3D divergence damping is indispensable to stabilize the split-explicit approach. In contrast, divergence damping is not essential for stability in ICON (however, to calculate diffusion on the longer fast physics time step, a weak 3D and 2D divergence damping is used, too). On the other hand, ICON needs a mechanism to stabilize artificial modes that arise due to the C-grid discretization on triangles. Here, a higher order

velocity reconstruction solves the problem (Zängl et al., 2015). Furthermore, additional fourth order hyperdiffusion and Smagorinsky diffusion are applied in both models mainly to suppress non-linear instabilities. However, the detailed strength of these mechanisms may be differently implemented in both models.

Finally, although not directly part of the Euler solver, the tracer advection schemes should be compared. COSMO uses the second order Bott (1989) scheme for the transport of the water variables and turbulent kinetic energy (Förstner et al., 2006), and potentially also for other variables e.g. arising in the ART module. Although this scheme is mass-conserving, this property is unfortunately slightly weakened due to a mass-consistency fix, which is needed for a proper moisture treatment (see also the discussion in Baldauf (2019)). ICON uses the third order scheme by Miura (2007) for the transport of water vapour ρ_v, and the corresponding second order variant for the other tracers. This scheme is mass-conserving, too, for every single tracer. The additional mass-consistency does not destroy mass-conservation because ICON itself is already mass-conserving.

These whole bundles of different discretization strategies make it quite difficult to answer in advance which dynamical core is superior over the other. Only a comprehensive simulation study with several tests can try to assess and compare these approaches.

3 Idealized test cases

In this main section, several idealized test cases that are relevant for small-scale models are performed. During the last decades, a certain set of such standard test cases for the non-hydrostatic flow regime has been established in the community of dynamical core developers for atmospheric models. These include linear wave expansion, linear and nonlinear flows over mountains, and highly nonlinear falling or rising of bubbles to test the solver for the Euler equations. These tests are designed to indicate e.g. possible problems with the terrain-following coordinate or with well-balancing properties. Additionally, there exist several test cases for the pure tracer advection.

Since the focus of the project lies on the capability of limited-area modeling, all tests use flat domains (i.e. they are not defined on a sphere). Technically, mainly the use of the alternative torus grid generator (by Leonidas Linardakis) instead of the standard ICON grid generator is a new aspect. It allows the use of either single periodic BCs (in y-direction only) of of double periodic BCs (in both x- and y-direction). Most of the test cases use a 2D $x-z-$ vertical slice setup. To this purpose four (double) rows of triangles with periodicity in y-direction have been placed along the 'equator' (along the x-axis) of the torus grid (side remark: two (double) rows of triangles should be sufficient to achieve periodicity, but a few internal calculations of metric coefficients require a larger grid).

A comparison by idealized test cases seems to be a very objective evaluation method. Nevertheless, some ambiguities remain; some broader discussion about such an evaluation can be found in Theis and Baldauf (2019). In the case of ICON and COSMO especially the different horizontal grids (triangle and quadrilateral, respectively) complicates the comparison of accuracy and efficiency. Whereas in COSMO Δx, Δy and Δz are just given by the quadrilateral dimensions of each grid cell, we use here for ICON Δx as the length of those triangle edge that goes around the 'equator' of the torus grid. Note, that in contrast Zängl et al. (2015) define the ICON grid spacing as the square root of the average grid cell area $\Delta x_A = \sqrt{\overline{A}}$. The difference is just $\sqrt{\overline{A}} \approx 0.658 \Delta x$. In COSMO, the time step Δt means the advective time step, whereas the fast waves time step is a factor of 6 smaller. In ICON, Δt denotes the 'fast-physics' time step, whereas the dynamics time step is a factor of 5 smaller.

For most of the idealized tests the COSMO version 5.4b.1 from 18 July 2016 was used and for ICON a version around September 2016. At this time the ICON dynamical core was settled enough and didn't changed since then. Nearly all tests have been performed on the Cray XC40 (Broadwell) at DWD, with the exception of the Weisman, Klemp-Test of section 3.6 performed on the operational Linux cluster (Sandy Bridge) at IMGW.

3.1 Linear gravity and sound wave expansion

This test case considers the expansion of gravity and sound waves, which are generated by the small vertical oscillations of a weak warm bubble in a stably stratified atmosphere, possibly with a horizontal background flow of constant velocity. The whole configuration is limited to a 2D channel with the horizontal length L and the height $H = 10$ km. Consequently, the test exercises every term of the Euler equations (but with the exception of all terrain-following metric correction terms) together with the time integration scheme. This setup was originally proposed by Skamarock and Klemp (1994), who delivered an approximated analytic solution. Later on, the test was slightly modified by Baldauf and Brdar (2013), in particular by using an isothermal background atmosphere with constant T_0, with the goal to deliver an (apart from linearization) unapproximated analytic solution. With such an analytic solution convergence properties can be investigated.

The test is performed in two setups: a 'small scale' setup with channel length $L = 300$ km, where all Coriolis terms have been switched off, and a 'large scale' setup with $L = 6000$ km and with Coriolis terms. Both tests use a background temperature of $T_0 = 250$ K.

3.1.1 Small scale test

Fig. 1 demonstrates the expansion of the wave pattern after 30 min. for the variables $T - T_0$ and w. The bubble initially was set in $x = 100$ km, and the whole field is advected by a constant background velocity of 10 m/s to the right. The comparison with the analytic solution of Baldauf and Brdar (2013) (blue lines) shows a good agreement already for the coarse horizontal grid spacing of $\Delta x = 1000$ m and an even better one for the finer grid spacing $\Delta x = 250$ m.

This convergence behavior is further examined in a dedicated convergence study shown in Fig. 2, which compares the standard error measures L_1, L_2, and L_∞ of the simulation against the analytic solution. Simulations with grid spacings of $\Delta x = \Delta z = 2000, 1000, 500, 250, 125$ m have been performed. COSMO used time steps of $\Delta t = 10, 5, 2.5, 1.25, 0.625$ s, respectively, and ICON used $\Delta t = 6, 3, 1.5, 0.75, 0.375$ s, respectively. Both models converge in all measures and both variables $T - T_0$ and w, however the convergence rate of COSMO is clearly below second order for w, and nearly second order for T only for coarser resolutions. In contrast, ICON shows an almost perfect second order convergence. An explanation for the slightly reduced convergence of COSMO due to the split-explicit approach is given in Baldauf (2010) (as a side remark: the convergence rate of COSMO shown in Baldauf and Brdar (2013) is even smaller. The reason was, that the distance for the application of periodic BCs was unfortunately chosen slightly smaller than $L = 300$ km; this happened due to the special treatment of periodic BCs in COSMO).

One should mention, that the second order convergence of ICON is only achievable, if the off-centering parameters in the vertically implicit integration are set to zero (i.e. a purely centered Crank-Nicholson scheme). This is not possible in the combination with physical parameterizations due to stability problems.

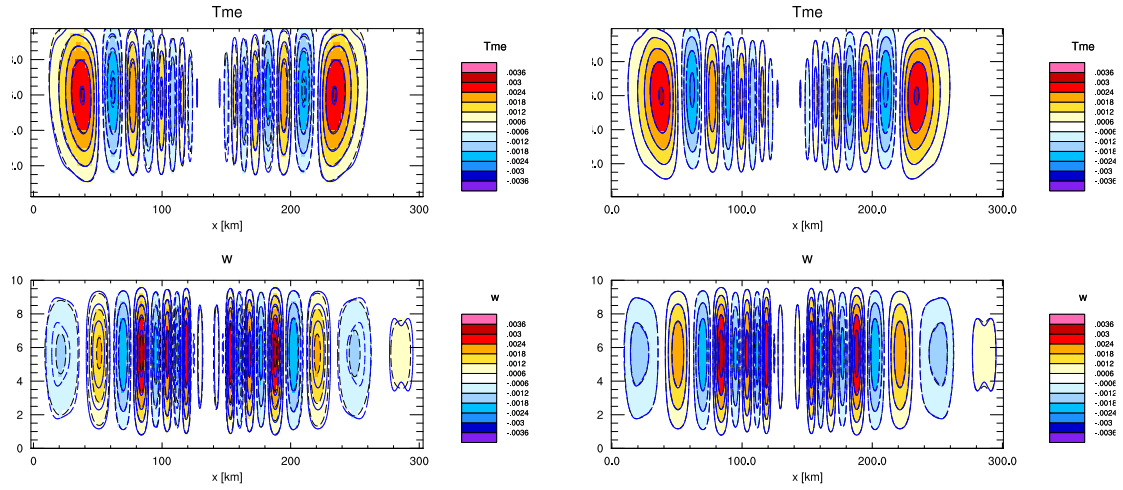

Figure 1: Linear gravity and sound wave expansion test. Small scale setup. COSMO simulation (colors and dashed, black, lines) after $t = 30$ min. Temperature deviation T' from background state (top) and vertical velocity w (bottom) for the grid spacing $\Delta x = \Delta z = 1000$ m (left) and $\Delta x = \Delta z = 250$ m (right). Analytic solution in blue lines.

3.1.2 Large scale test.

In the large scale test, the background velocity is set to zero; this is necessary for the proper comparison with the analytic solution in the case of a non-vanishing Coriolis force. Fig. 3 shows the wave pattern after 8 hours for the variables $T - T_0$ and w. In this large scale setup both models show a proper second oder convergence (Fig. 4), with slightly smaller errors for ICON (however, this also depends on a proper definition of grid spacing in ICON, see above).

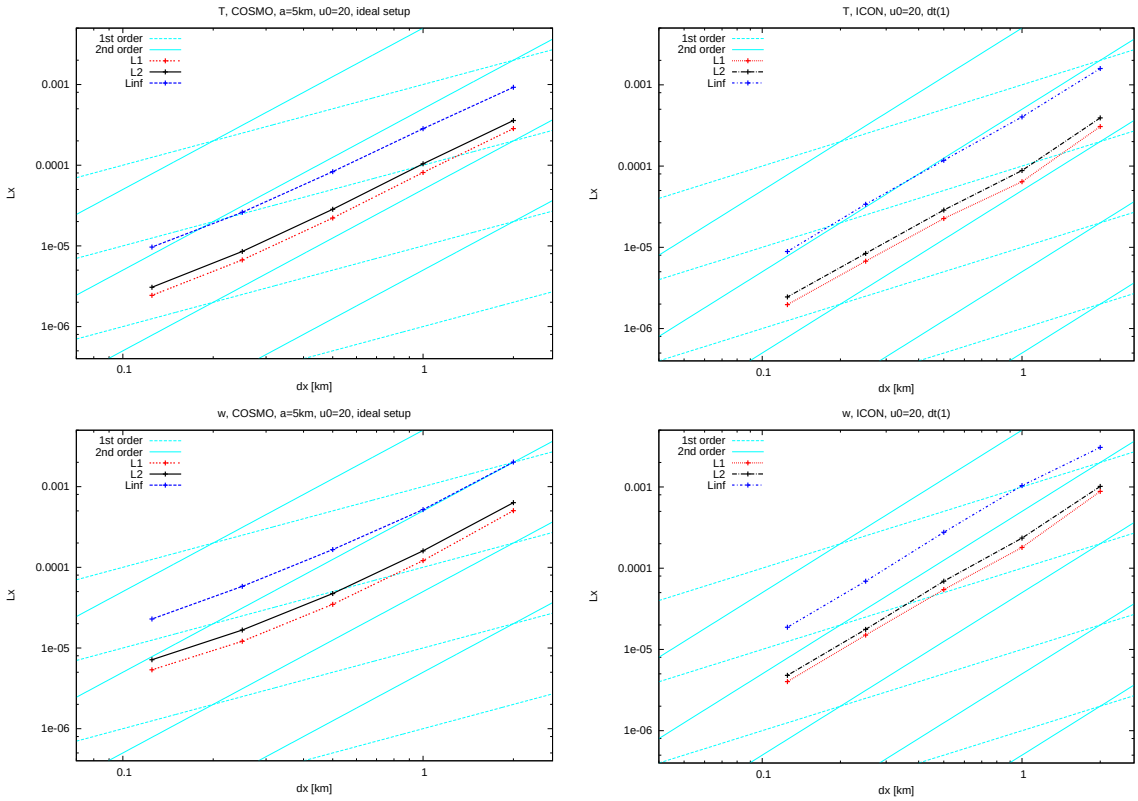

Figure 2: Linear gravity and sound wave expansion test. Small scale setup. Error measures L_1 , L_2 and L_∞ over the grid spacing for temperature deviation T' from background state (top) and vertical velocity w (bottom). Comparison between COSMO (left) and ICON (right).

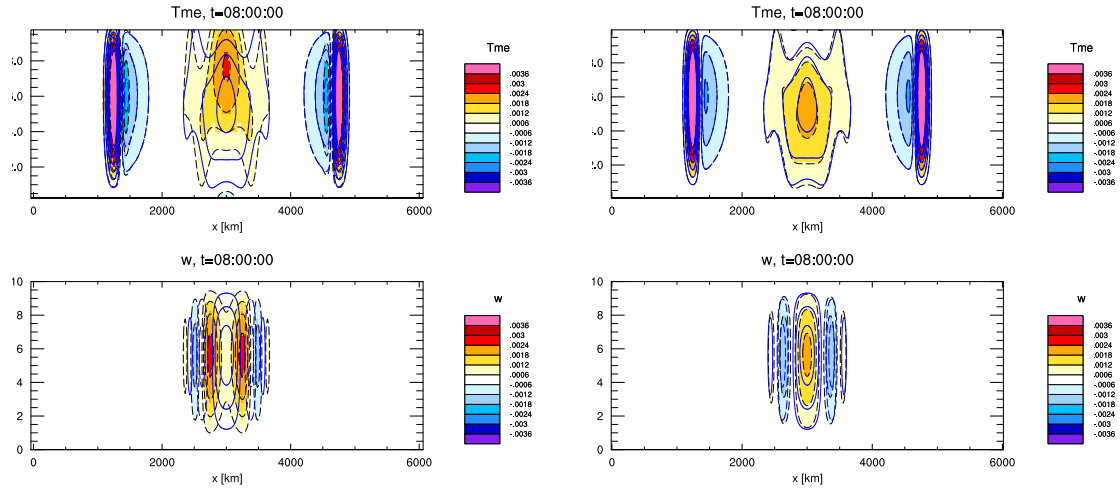

Figure 3: Linear gravity and sound wave expansion test. Large scale setup. COSMO simulation (colors and black, dashed lines) after $t = 8$ h. Temperature deviation T' from background state (top) and vertical velocity w (bottom) for the grid spacing $\Delta x = 20$ km (left) and $\Delta x = 5$ km (right), and $\Delta z = \Delta x/40$. Analytic solution in blue lines.

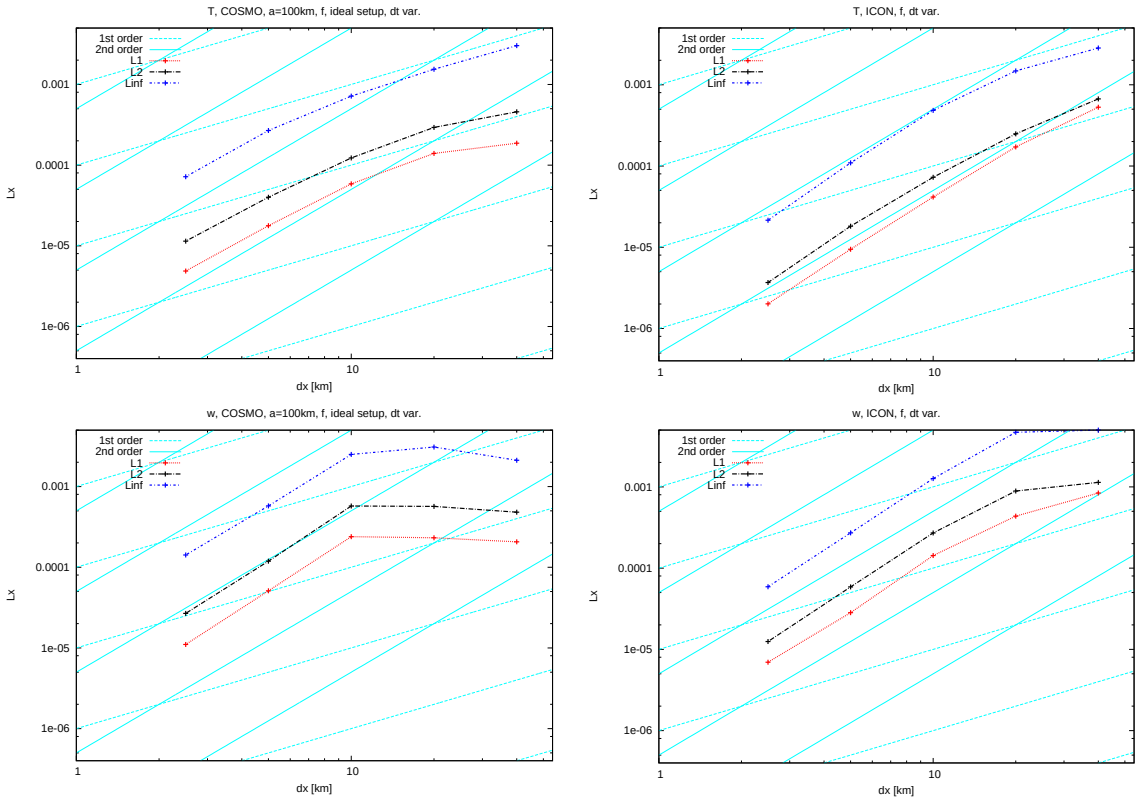

Figure 4: Linear gravity and sound wave expansion test. Large scale setup. Error measures L_1 , L_2 and L_∞ over the grid spacing for temperature deviation T' from background state (top) and vertical velocity w (bottom). Comparison between COSMO (left) and ICON (right).

3.2 Atmosphere at rest

This test consists of a single mountain of Gaussian shape with a maximum height of 1000 m and a half width of 5000 m analogous to Zängl et al. (2004). The atmosphere is at rest with a prescribed stratification with constant Brunt-Vaisala frequency of $N = 0.01$ 1/s and a temperature of $T = 288$ K at mean sea level. The other thermodynamic variables are in hydrostatic balance. Such a configuration should remain stationary for arbitrarily long times. However, at least for models that use terrain-following coordinates, a numerical imbalance between differently discretized terms will induce a flow after some time. Obviously, as smaller these disturbances are, as better the model formulation. In principle, this test cases inspects two properties of the model: first, the accuracy of the pressure gradient in vertical direction and along coordinate surfaces and its balance with the buoyancy term. Second, it tests the accuracy of the initial hydrostatic balance (a piecewise polytropic atmosphere was initialized and the new exponential reference atmosphere was used in both models). A further discussion about this test case can be found in Zängl et al. (2004).

Figure 5 demonstrates that ICON (bottom) induces much less disturbances than the standard setup of COSMO (top): COSMO induces vertical velocities w that reach about ± 4 m/s, whereas ICON induces maximum values of less than ± 1 m/s and spatially more limited to the vicinity of the mountain. Both models use the same vertical grid spacing, relatively close to operational settings ($\Delta z \approx 19.8$ m near the bottom until 780 m at the model top). After about 17 hours, the COSMO run broke. One can reduce the disturbances of COSMO and prevent the model crash by using third order implicit vertical advection. However, this version decouples the vertical advection process a bit more from the other dynamical processes and therefore was never used operationally.

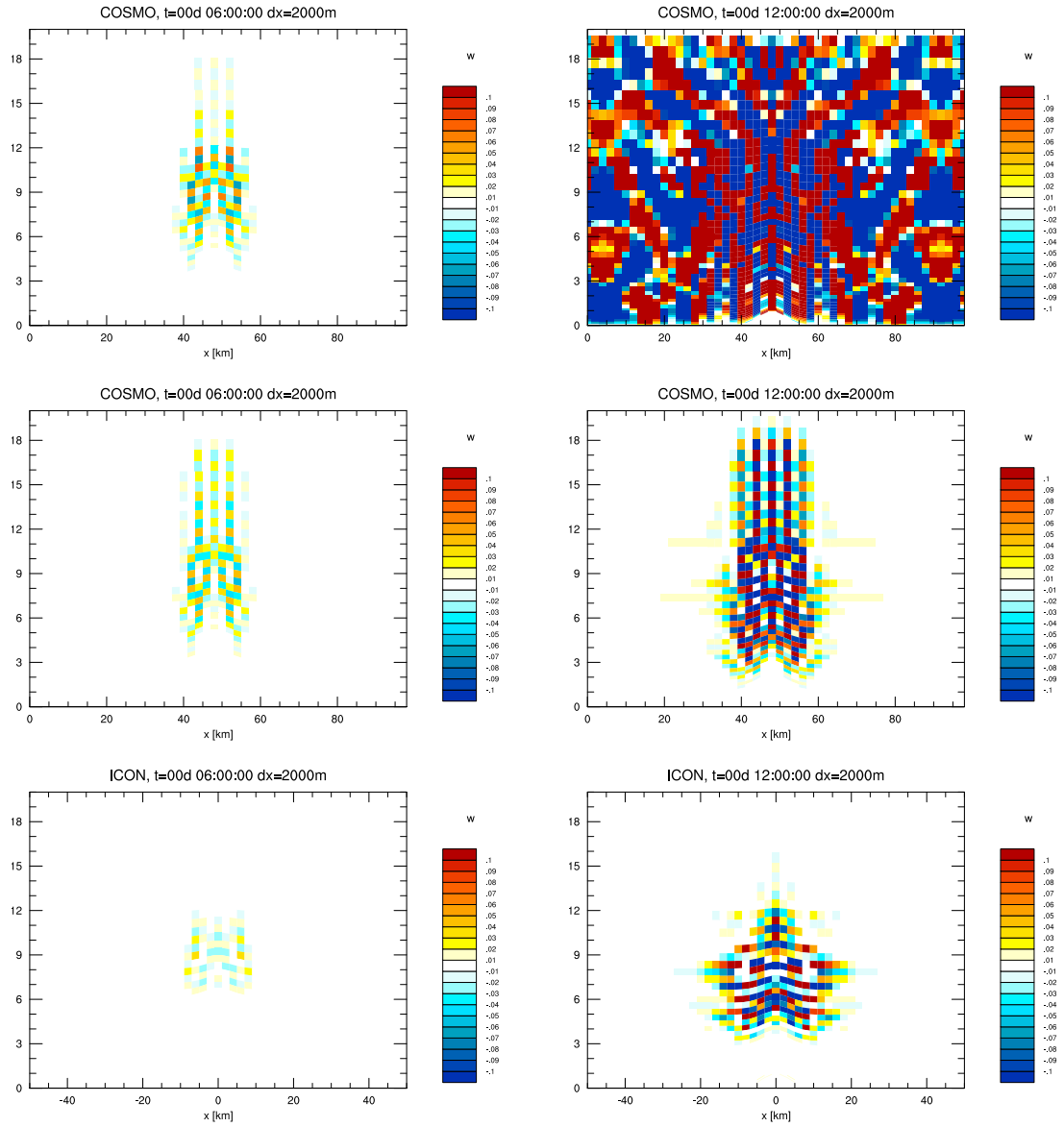

Figure 5: Atmosphere at rest. COSMO with operational setting (top), COSMO with third order vertical implicit advection (middle), and ICON (bottom). w after $t = 6$ h (left) and 12 h (right).

3.3 Linear flow over mountains

A further standard test case is the linear flow over flat mountains. Such a test investigates many of the spatial discretizations of a model including the metric terms of the terrain-following coordinate formulation. Their correct implementation and numerical behavior again can be assessed by the comparison with the linearized analytic solution, which is applicable due to the quasi-linearity of the setup. Here, the analytic solution of Baldauf (2008) is used, which is virtually identical to the slightly more approximated solution by Smith (1980).

The whole setup is adapted from Schär et al. (2002) (section 5b), which defines a series of mountains with the orography function

$$h(x) = H_0\, e^{-x^2/a_e^2}\, \cos^2 \pi \frac{x}{a_c}$$

with the two length scales $a_e = 5$ km and $a_c = 4$ km. The inflow velocity is $u_0 = 10$ m/s, the temperature is stably stratified with a constant Brunt-Vaisala frequency of $N = 0.01$ 1/s, and the surface temperature is $T_s = 288$ K.

3.3.1 2-dimensional flow

The vertical grid is chosen as equidistant. The maximum mountain height is $H_0 = 25$ m, which results in a vertical Froude-number of $Fr_H = u_0/(NH_0) = 40 \gg 1$. Therefore, this setup can be considered as linear in a good approximation. The horizontal Froude-number $Fr_a = u_0/(NL)$ lies in the range 0.1...0.5, i.e. in the range of almost hydrostatic to nearly non-hydrostatic flow over mountains. As can be seen in Fig. 6, both models reproduce the analytic solution quite well, perhaps with a minimal advantage for ICON. Note, that a proper convergence study is difficult due to the influence of the artificial damping layers and therefore was not performed (this problem does not exist in the test case of section 3.1). Beyond this, both models use different formulations: whereas COSMO uses a relaxation scheme towards the large scale values for all prognostic variables, ICON uses the damping layer formulation for w alone by Klemp et al. (2008). At least, a comparable damping height starting in about $z = 14$ km was used both in COSMO and ICON.

3.3.2 3-dimensional flow

The setup for the 3D flow uses a vertically stretched grid with a cell thickness of 24.7 m near the ground and 976 m at the model top. This vertical grid spacing and the background temperature profile is shown in Fig. 7. For the horizontal grid spacing the coarser value $\Delta x = 500$ m has been chosen for these 3D simulations. Now a circular symmetric Gaussian mountain $h(x, y) = H_0\ 2^{-(x^2+y^2)/a^2}$ is used with $H_0 = 1$ m (leading to $Fr_H = 2000$) and $a = 5$ km (leading to $Fr_a = 0.4$). The inflow velocity is $u_0 = 20$ m/s and the stratification again uses a constant $N = 0.01$ 1/s. The damping layers are chosen as for the 2D case, and Fig. 8 demonstrates that both damping layers behave relatively similar near the model top. Both models reproduce the analytic solution quite well (Fig. 9), now perhaps with a minimal advantage of COSMO. This demonstrated in particular that all metric correction terms are correctly implemented in both models.

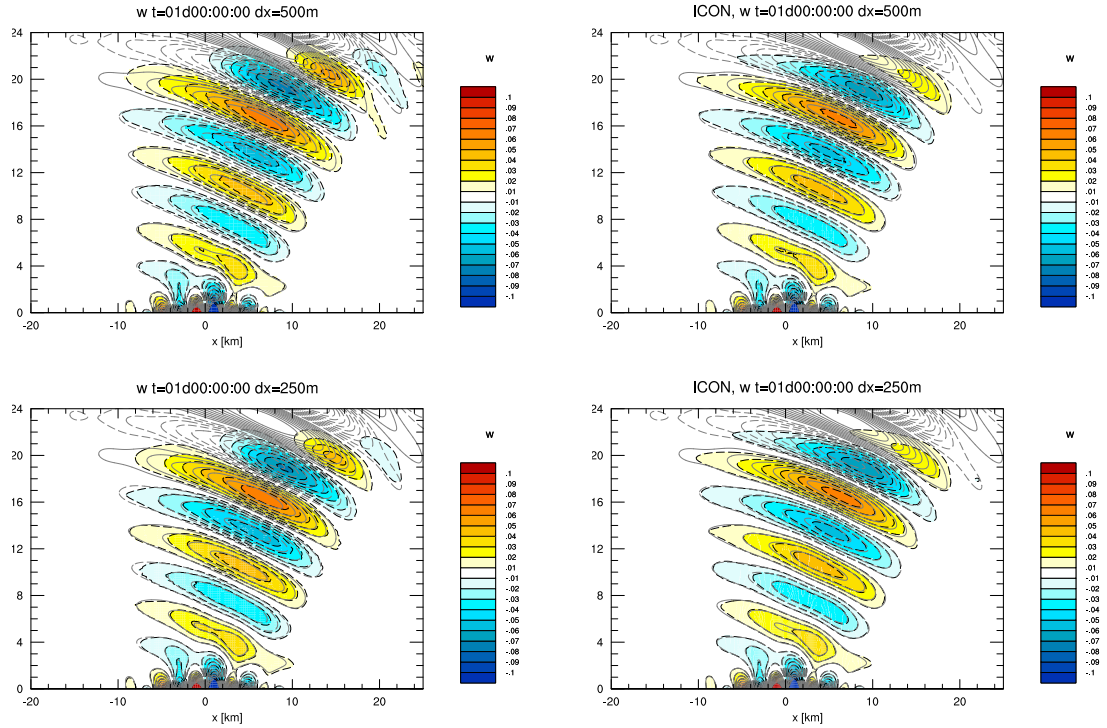

Figure 6: 2D linear flow over mountains. Vertical velocity w of COSMO (left) and ICON (right) for the two resolutions $dx = 500$ m (top) and $dx = 250$ m (bottom). Colors and dashed, black lines: simulation; grey lines: analytic solution.

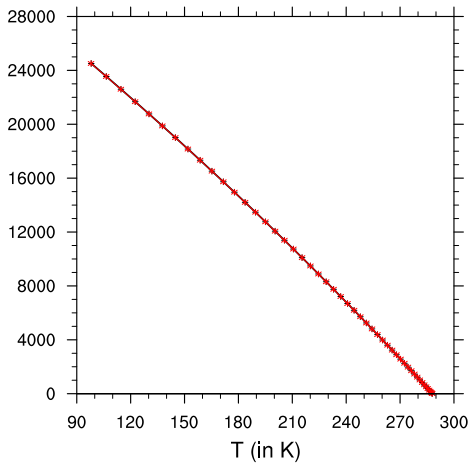

Figure 7: 3D linear flow over mountains. Initial temperature profile and vertical grid spacing (stars).

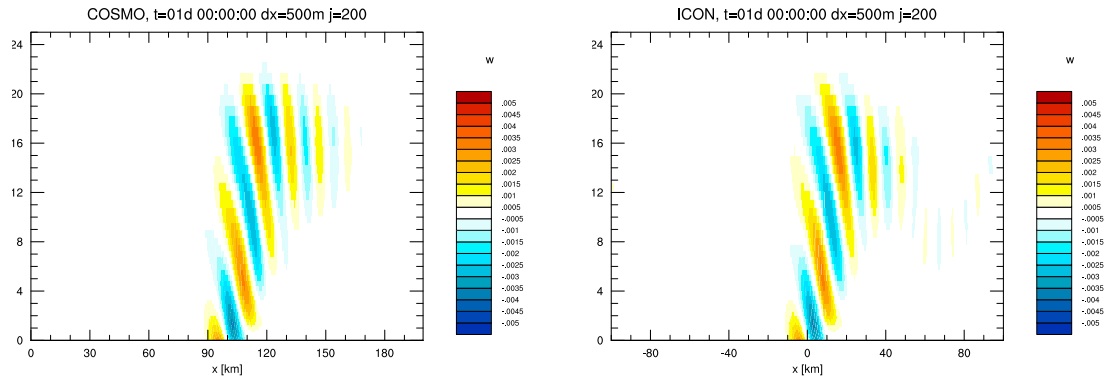

Figure 8: 3D linear flow over mountains. COSMO (left) and ICON (right). Vertical cross section of vertical velocity w through the symmetry axis.

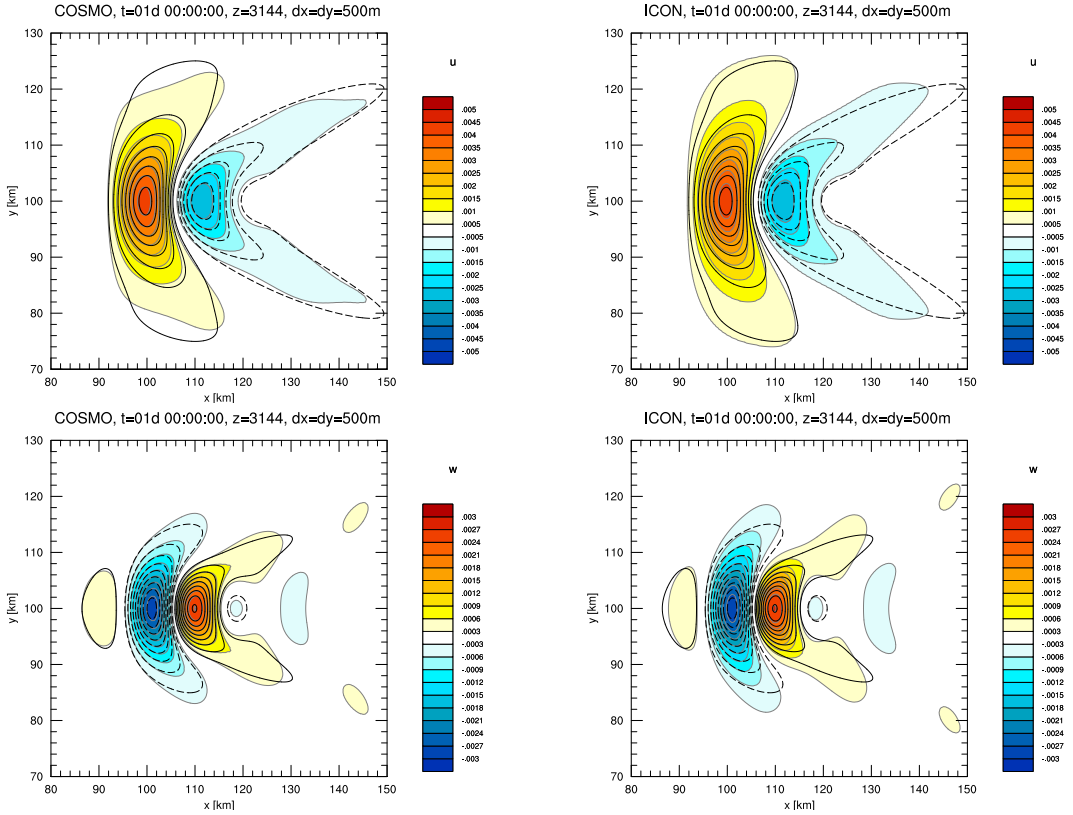

Figure 9: 3D linear flow over mountains. COSMO (left) and ICON (right). Horizontal cross sections of horizontal velocity u (top) and vertical velocity w (bottom) at height $z = 3144$ m above MSL. Colors and grey lines: simulations; black lines: analytic solution.

Table 1: Some characteristic values for the Gaussian mountain $h(x, y) = H_0\ 2^{-(x^2+y^2)/a^2}$ with $a = 3$ km in the 3D non-linear case: the maximum mountain height H_0, the maximum orography step max Δh between two neighboring grid cells, and the maximum slope angle max α.

H_0	max Δh	max α
1000 m	234.9 m	13.2°
3000 m	704.7 m	35.2°
4000 m	939.6 m	43.2°
4500 m	1057 m	46.8°
4700 m	1104 m	48.0°
5000 m	1174 m	49.6°
6000 m	1409 m	54.8°
7000 m	1644 m	58.9°
8000 m	1879 m	62.0°

3.4 Nonlinear flow over steep mountains

We use the same setup as for the linear 3D flow in section 3.3.2, with the exception that the Gaussian mountain is bit narrower ($a = 3$ km) and the mountain heights H_0 are much higher to reach the strongly non-linear regime with steep mountains. Furthermore, an even coarser horizontal grid spacing of $\Delta x = 1000$ m has been chosen to again increase the height step Δh between two neighboring grid points (the vertical grid stretching is the same as in section 3.3.2). Additional to the slope angle, Δh has a stability limiting influence, too. Table 1 gives some characteristic properties for these mountains and the setup. To prevent model breaks by unphysical gravity wave breaking, turbulent diffusion was switched on (each model uses its 'standard' turbulence scheme for this purpose).

Fig. 10 shows the comparison between COSMO and ICON for relatively moderate mountain heights up to $H_0 = 3000$ m. To keep the model domain small enough to perform larger series of tests, a periodic boundary condition has been chosen. Its effect is visible by the entrance of the mountain lee wave again on the left side of the domain. This might have a certain influence to the mountain inflow (e.g. some sort of blocking), however, these effects seem tolerable for this more qualitative study.

Fig. 11 shows the COSMO model for the maximum heights $H_0 = 4000$ m (in comparison with ICON), and 4500 and 4700 m. These COSMO simulations are only stable with the Mahrer discretization of the pressure gradient term (Baldauf, 2013).

Fig. 12 shows the ICON model for mountain heights H_0 between 5 km and 8 km; COSMO is no longer stable for such high values of H_0, whereas ICON tolerates very steep mountains. This very positive property is due to a modified version of the Mahrer discretization by Zängl (2012).

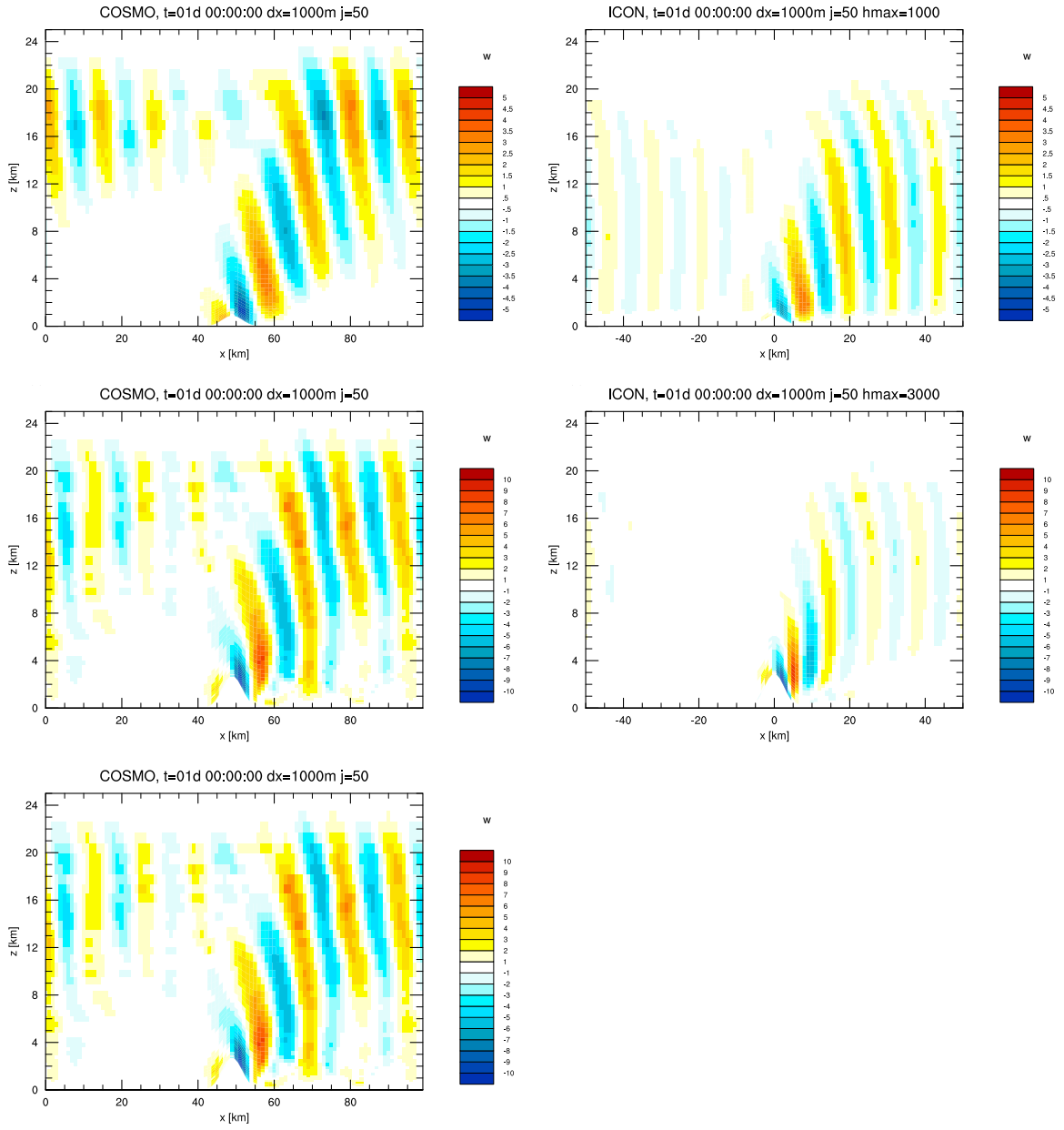

Figure 10: 3D flow over steep mountains. Cross section through the symmetry axis of COSMO (left) and ICON (right) for maximum mountain heights $H_0 = 1000$ (top) and $H_0 = 3000$ m. The bottom figure shows COSMO but with the alternative Mahrer-discretization in the fast waves solver.

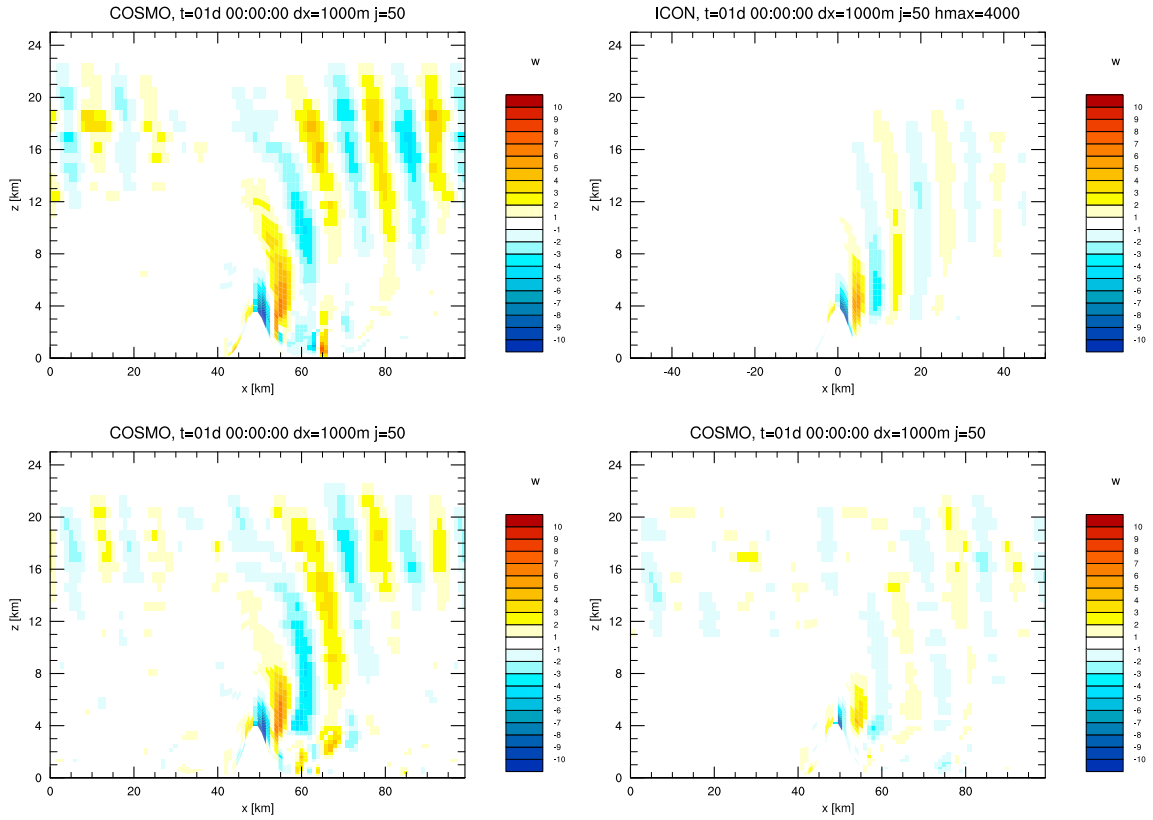

Figure 11: 3D flow over steep mountains, COSMO and ICON for maximum mountain heigh $H_0 = 4000$ (top row). COSMO for $H_0 = 4500, 4700$ m (bottom row).

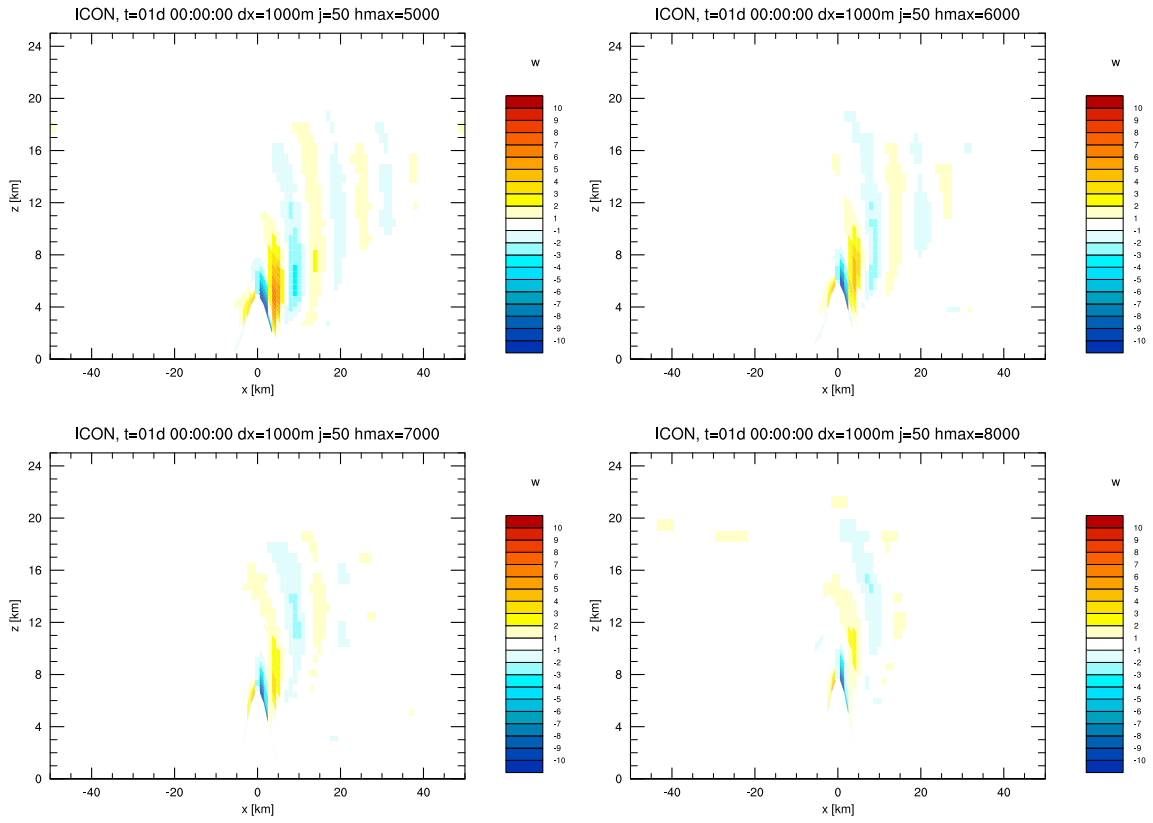

Figure 12: 3D flow over steep mountains with the ICON model for maximum mountain heights $H_0 = 5000$, 6000, 7000 and 8000 m (top, left to bottom, right).

3.5 Falling cold bubble

This highly non-linear test case is defined in Straka et al. (1993). A bubble that is up to 15 K colder than the neutrally stratified surrounding atmosphere is set 3 km above the ground in a 6.4 km high and 51.2 km wide 2D channel. This initial situation is shown in the left, upper panel in Fig. 13 (only a part of the right half of this horizontally symmetric setup is shown) The bubble falls down and after hitting the ground, bow fronts on both sides evolve. Due to a Kelvin-Helmholtz instability, several vortices are generated. To prevent the simulation to develop too fine-scale structures and to allow convergence, diffusion with a constant diffusion coefficient of $K = 75m^2/s$ is used both for heat and momentum. Coriolis force is switched off.

Fig. 13 shows the evolution of the potential temperature for the grid spacing $\Delta x = \Delta z = 25$ m with the COSMO model. For this fine resolution one can expect an almost converged solution; in fact the agreement with the reference solution given in Straka et al. (1993) (their Fig. 1) is very good (note that Fig. 13 and 14 use the same isolines as this reference figure).

Fig. 14 shows a comparison between COSMO and ICON for the different grid spacings $\Delta x = \Delta z = 200, 100, 50, 25$ m, where for COSMO time steps of $\Delta t = 2.0, 1.0, 0.5, 0.25$ sec. have been used, and for ICON $\Delta t = 1.44, 0.72, 0.36, 0.18$ sec., respectively. One easily recognizes the convergence of both models for finer resolutions. However, the final state of ICON (i.e. after 15 min.) is not exactly identical to the reference solution of Straka et al. (1993). (e.g. the second vortex overlaps the third one a bit more). Until now, the reason for this behavior is not yet clear. One only can speculate that the diffusion might work slightly different, but further investigation seems to be necessary.

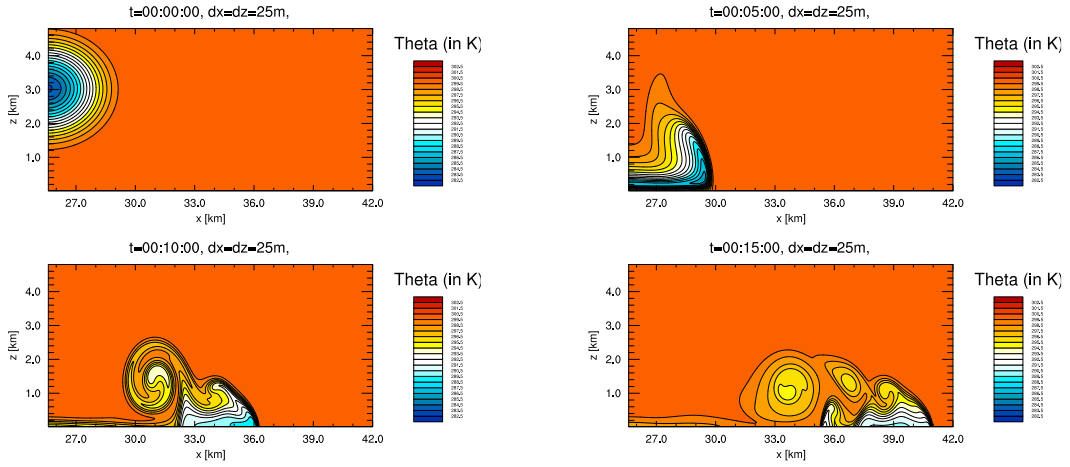

Figure 13: Falling cold bubble test. COSMO, $\Delta x = \Delta z = 25$ m, Θ after t=0, 5, 10, 15 min., `y_vert_adv_dyn='impl2'`. Only parts of the right half of the domain is shown.

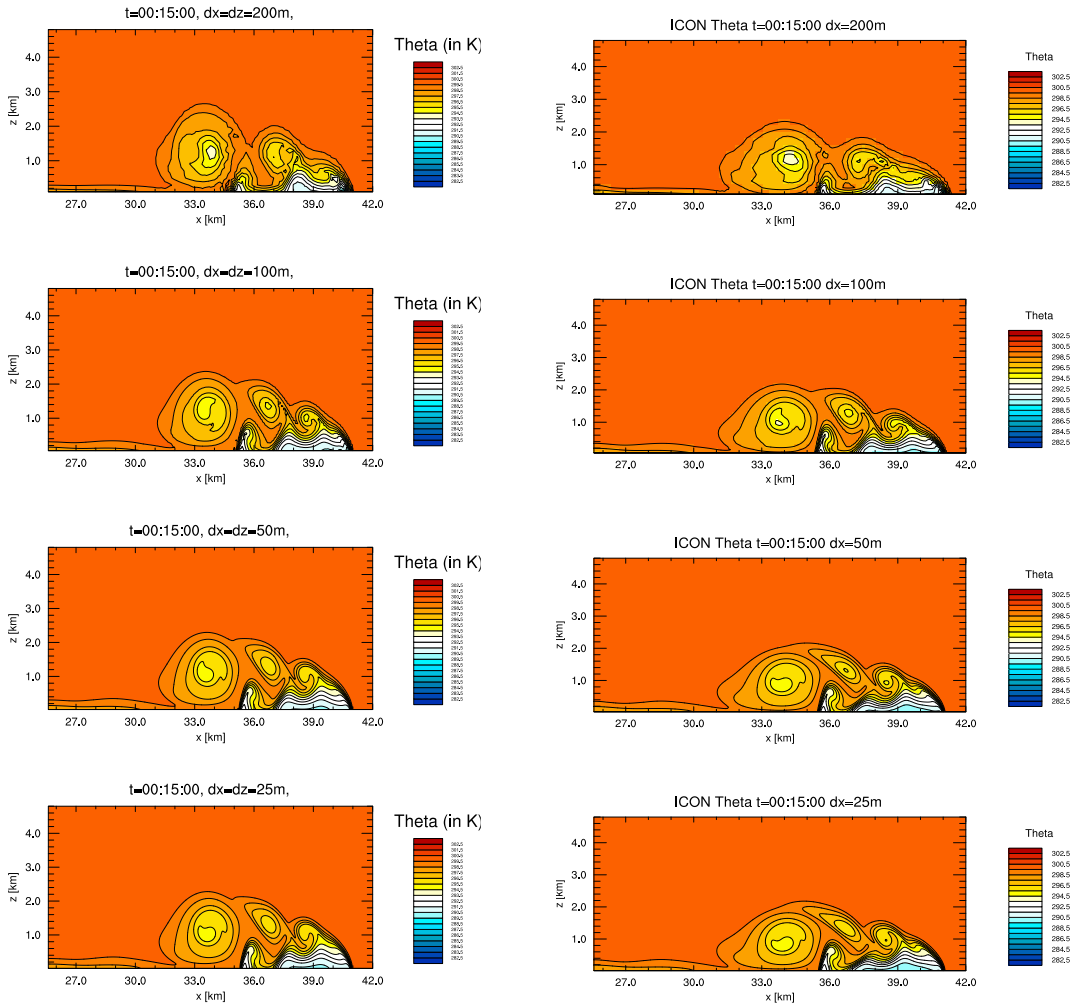

Figure 14: Falling cold bubble test. Θ after t=15 min., comparison between COSMO (left) and ICON (right) for different grid spacings $\Delta x = \Delta z = 200, 100, 50, 25$ m.

3.6 The Weisman and Klemp (1982) test case

This section reports results from the idealized moist deep convection test case of Weisman and Klemp (1982) carried out for the ICON model. The test requires from the model a capability to handle nonhydrostatic flows, triggered by latent heat release and rain water evaporation. The ICON model results are compared with references provided by the COSMO model (Baldauf et al., 2011) and Weisman and Klemp (1982) model. Symmetry of solutions allows limiting comparisons to the southern part of the computational domains.

3.6.1 Experimental setup

Definition of the environmental atmospheric profiles of potential temperature, moisture, and wind predominantly follows the setup of Weisman and Klemp (1982) (theirs Equations 1, 2, and 4). The qv_0 parameter of the moisture profile is set to 14 g/kg. Subsequent simulations differ by the environmental wind shear parameter U_S, while the other parameters are kept unchanged. A constant wind profile is added to the original environmental wind profile in the ICON simulations ($0.45 \cdot U_S$) to keep developing convective systems near the centre of the computational domain. Convection is initiated by an ellipsoidal thermal having the horizontal radius $r_h = 10$ km, vertical radius $r_v = 1.4$ km, and maximum temperature excess $+6°$C.

The computational domain of the ICON model utilizes a horizontally-unstructured grid equivalent to a cartesian 100 x 100 grid points periodic grid with the grid length equal 2 km. The vertically-structured grid has 90 levels, with stretching, and spans up to 40 km height above the surface. The sponge layer is between 25 km height and the top of domain. The simulations are carried out using a 3-category ice Kessler-like microphysical scheme, with snow, cloud ice, and graupel. The turbulence parameterization utilizes a TKE-based mixing scheme. The integration time is limited to 120 minutes. The Coriolis force is not included in the model equation set.

Configuration of the reference COSMO simulations is based on the ARTIFCTL module of Blahak (2015) and approximately follows the ICON model test case configuration. A few important differences are listed below:

- the horizontal grid of the COSMO model is structured,
- the original environmental wind profiles are used,
- the COSMO domain is elongated to 300 km in the X-direction,
- the vertically-structured grid has 74 levels between the surface and 25 km height, sponge layer starts at 15 km height, and levels are colocated with the ICON levels.

Data visualisation is based on the NCL environment[1]. The ICON native-output data were used for visualisation. Data regridding to the cartesian grid was carried out using tools the Earth System Modeling Framework[2] tools.

[1] www.ncl.ucar.edu

[2] www.earthsystemcog.org/projects/esmf/

3.6.2 Results of simulations

Three types of experiments were performed with the wind shear parameters (U_S) equal 15, 25, and 35 m/s. A few principal convective phenomena are observed in each simulation: (i) formation of an updraft in result of the convection initiation, (ii) formation of rain shafts, (iii) subsequent formation of precipitation-driven downdrafts, and (iv) a cold pool growth at the surface. For example, all these phenomena are observed in the ICON $U_S = 15$ m/s simulation (Figure 15), as well as in the reference Weisman and Klemp (1982) (Figure 16) and COSMO (Figure 17) simulations.

Growth of 4 convective cells is observed in the low-shear ICON simulation ($U_S = 15$ m/s; Figure 15). Those cells live relatively short and feature relatively moderate vertical velocities and vorticity within the mid-tropospheric updrafts (Figure 15 and Figure 18, left). That suggests that those cells are likely not supercellular.

Convective cells that develop at the gust front in the ICON simulation with $U_S = 15$ m/s (e.g., cell II) tend to move slower than the gust front and are prone to decay once cut off from CAPE-rich air. A qualitatively similar solution is observed in Weisman and Klemp (1982) (Figure 16). A rather contrasting solution is observed in the COSMO simulation (Figure 17). In that simulation, a long-lived cell develops with a stronger updraft encompassing increased vertical vorticity (around 0.006 s^{-1} in the COSMO versus 0.004 s^{-1} in the ICON; Figure 19, left), and that cell sticks to the gust front.

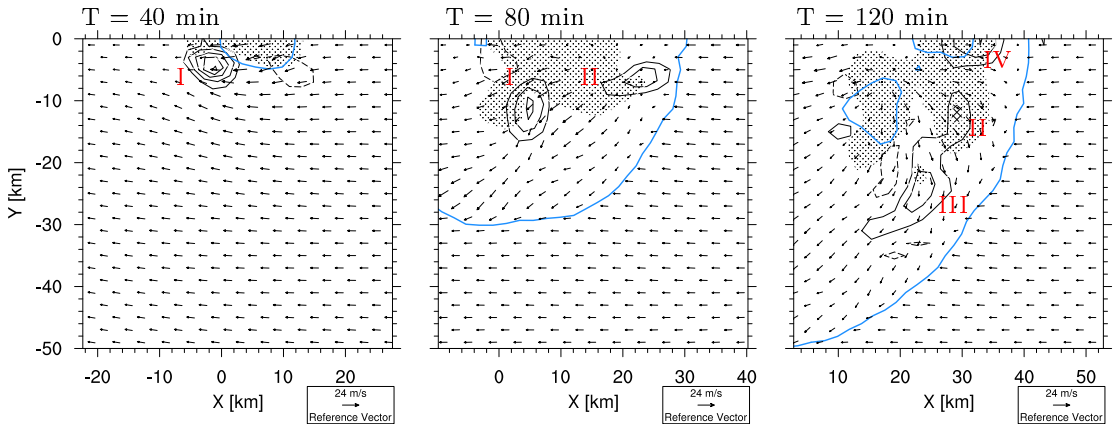

Figure 15: Convective cells and low-level flow field developing in the ICON simulation with $U_S = 15$ m/s. The arrows denote approximately storm-relative flow at 147 m height above the surface ($\overline{U} = 12$ m/s was subtracted from the flow field). The blue line denotes the meso-cold front position at 10 m height. The contours denote vertical wind speed at 4677 m height (contours shown for -8, -6, -4, -2, 5, 10, 15, 20, 25, 30 and 35 m/s; negative values dashed). The shading (hatching) denotes the rain water mixing ratio exceeding 1 g/kg (4 g/kg) at 10 m height. Individual convective cells are marked with the red roman numbers.

The ICON simulation with $U_S = 25$ m/s is shown in Figure 20. Here, two convective cells develop by 80 minute of simulation and subsequently merge around 120 minute. At least three differences arise in comparison to the previous ICON simulation. First, the mid-level vertical vorticity within the first cell (I) reaches around 0.008 s^{-1} (Figure 18, middle), that is, a value close to the threshold defining the mid-level supercellular mesocyclone (0.01 s^{-1}). Second, the cell I is long-lived and has a rather compact updraft. Finally, the cell I propagates around 36 km to the south after 120 minutes of simulation. Those observations suggest that the cell I represents to some extent the supercellular convection. A quite similar convective

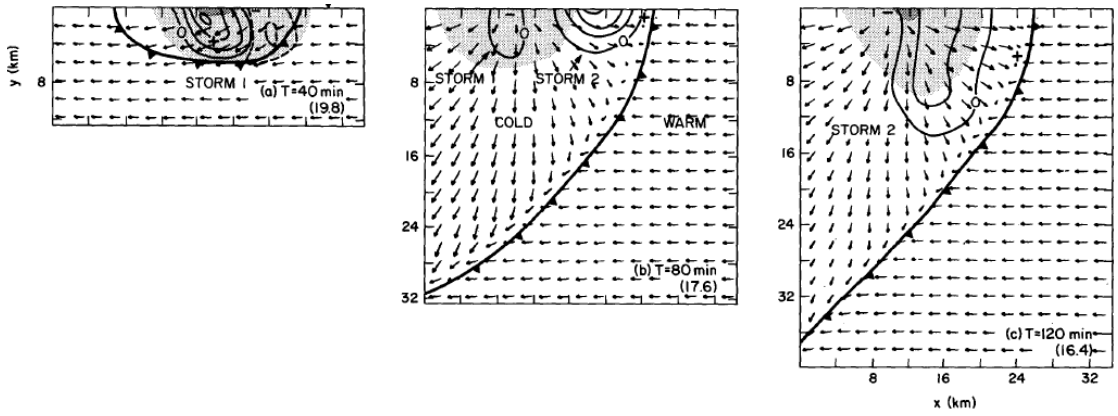

Figure 16: The reference Weisman and Klemp (1982) simulation for $U_S = 15$ m/s (theirs Figure 4).

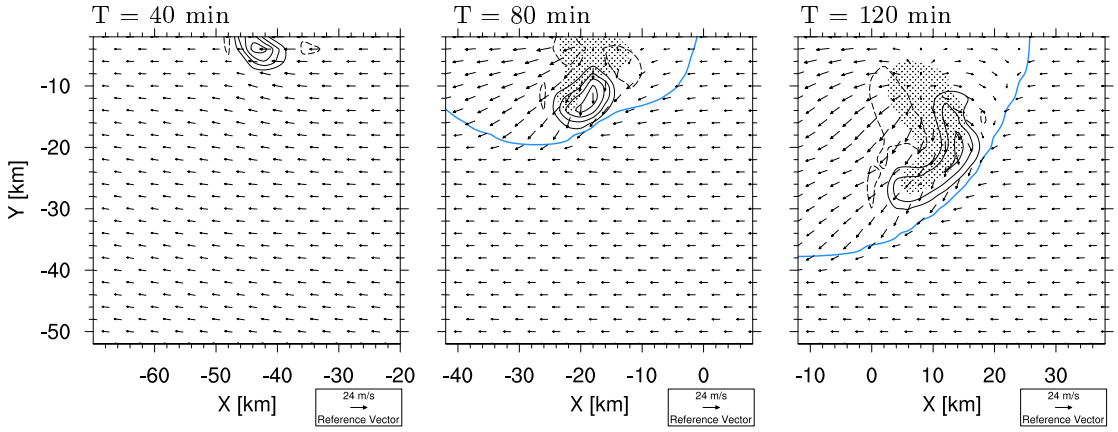

Figure 17: The reference COSMO simulation with $U_S = 15$ m/s, and $\overline{U} = 12$ m/s. Data is depicted as in Figure 15.

cell with the vertical vorticity of around 0.008 s^{-1} (Figure 19, middle) is observed in the COSMO simulation as well (Figure 21).

Figure 22 shows a convective cell developing in the ICON simulation with the strongest environmental wind shear ($U_S = 35$ m/s). At 80 minute, the maximum mid-level vertical vorticity of the cell exceeds 0.012 s^{-1} (Figure 18, right), a value in the range of supercellular mesocyclones. The cell moves to the right of the environmental winds and departs around 42 km to the south (120 minute), while remaining in proximity of the gust front. The updraft and precipitation shafts seem to be almost separated. Therefore, that cell likely represents the supercellular convection. The reference COSMO (Figure 23 and Figure 19, right) and Weisman and Klemp (1982) simulations (Figure 24) show development of quite similar supercellular storms. In those simulations, the maximum vertical vorticity is slightly weaker (around 0.008 s^{-1} and 0.01 s^{-1}, respectively).

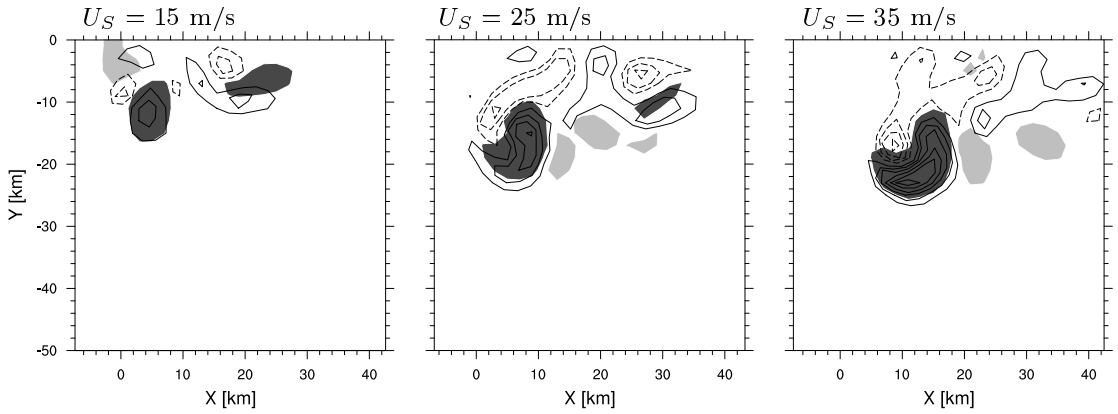

Figure 18: Vertical vorticity at 4677 m height (negative values dashed; contour interval 0.002 s^{-1}; the zero contour not shown) after 80 minutes of the ICON simulations. Light (dark) shading denotes vertical velocities lower than −2 m/s (larger than 5 m/s) at the same height.

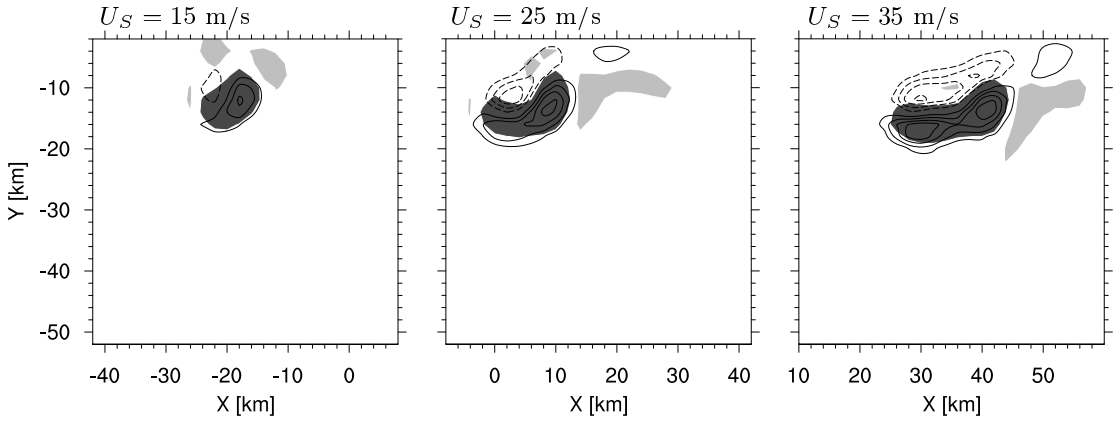

Figure 19: Vertical vorticity at 4677 m height (negative values dashed; contour interval 0.002 s^{-1}; the zero contour not shown) after 80 minutes of the COSMO simulations. Light (dark) shading denotes vertical velocities lower than −2 m/s (larger than 5 m/s) at the same height.

3.6.3 Summary

This experiment was intended to verify whether the nonhydrostatic ICON model is capable to simulate deep moist convective flows, and in particular the supercellular convection. Although the scope of analysis was limited, results indicate that this model consistently simulates convective flows in differently-sheared environments. The long-lived supercellular convection begins to develop in the moderate-shear environment and is further enhanced in the large-shear environment. When evolution of morphological flow features is concerned, convection observed in the ICON simulations is more similar to the one in the Weisman and Klemp (1982) simulations than in the COSMO simulation (especially for the low-shear experiment). The results do not indicate presence of any basic error in the coupling between the ICON nonhydrostatic dynamical core, saturation adjustment scheme, and parameterizations of the moist and turbulent processes.

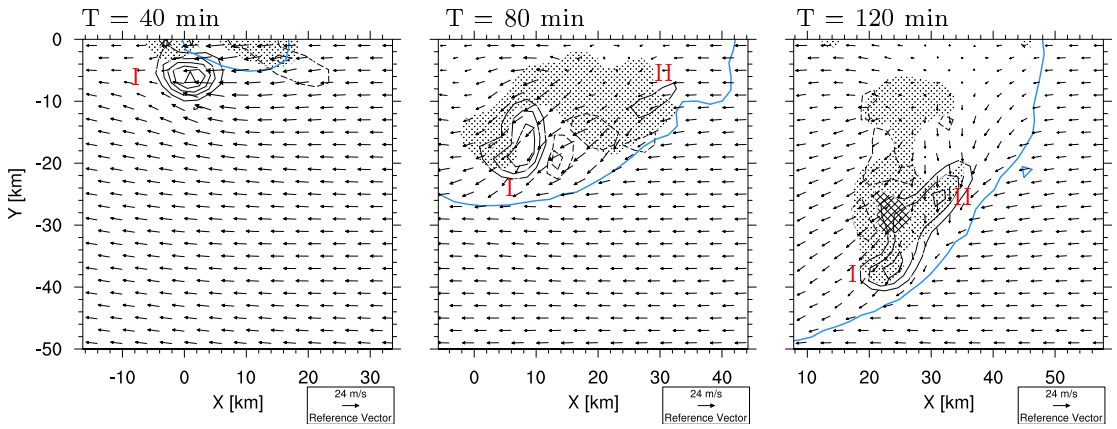

Figure 20: As Figure 15 but for the $U_S = 25$ m/s, and $\overline{U} = 19$ m/s.

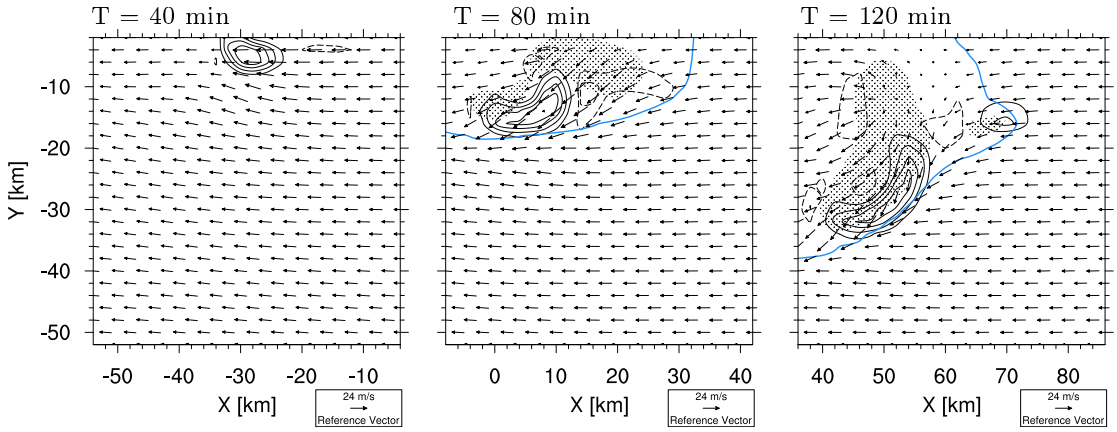

Figure 21: As Figure 17 but for the $U_S = 25$ m/s, and $\overline{U} = 19$ m/s.

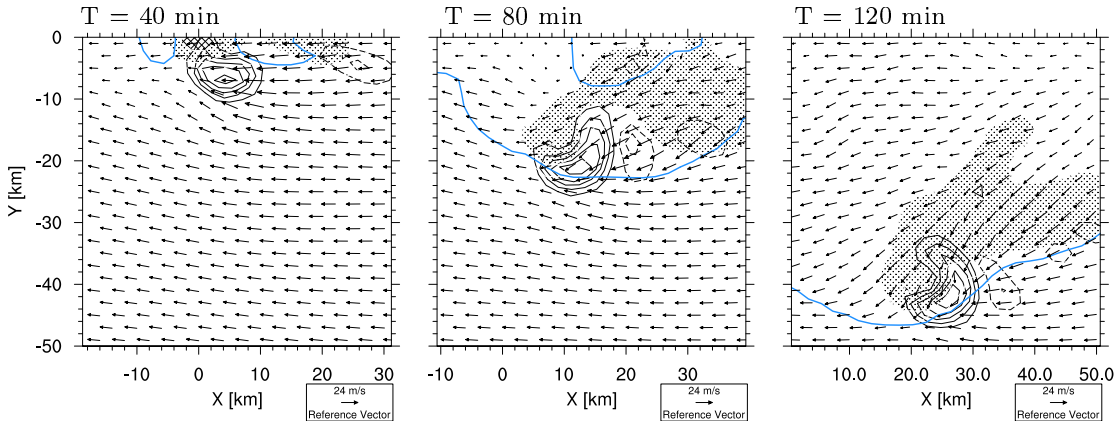

Figure 22: As Figure 15 but for the $U_S = 35$ m/s, and $\overline{U} = 22.5$ m/s.

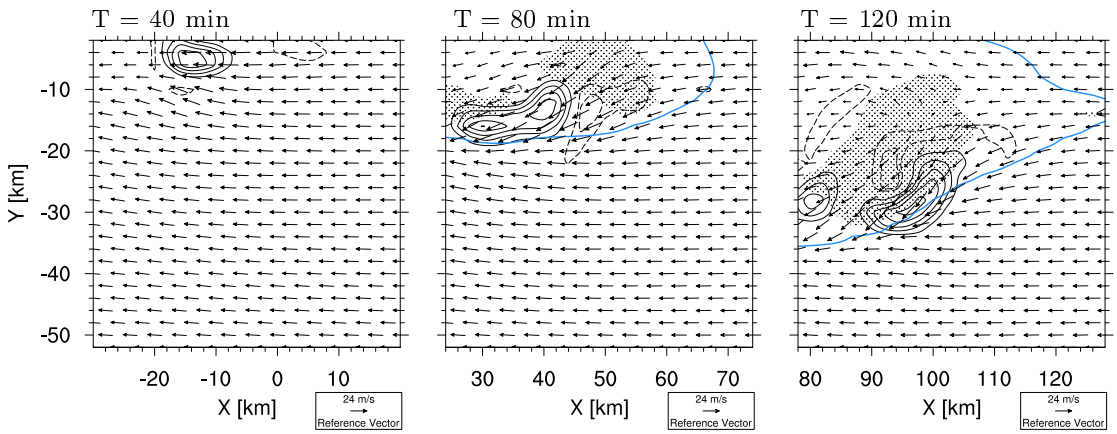

Figure 23: The reference COSMO simulation with $U_S = 35$ m/s, and $\overline{U} = 22.5$ m/s. Data is depicted as in Figure 15.

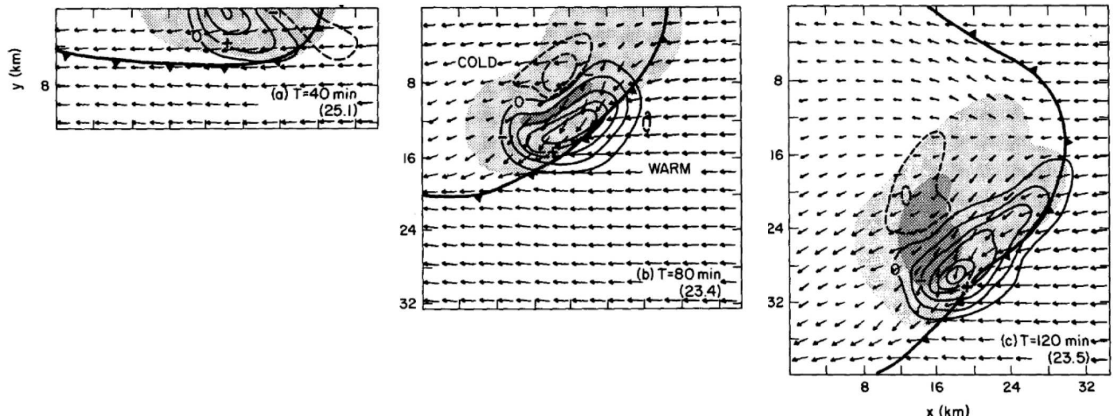

Figure 24: The reference Weisman and Klemp (1982) simulation for $U_S = 35$ m/s (theirs Figure 6).

4 Scalability aspects

In such a basic comparison between two models, computational efficiency of course also plays a big role. In general, one can say, that ICON runs definitely faster than COSMO on most platforms. In this section, we want to investigate in particular the scaling behaviour of both models for larger numbers of processors on massively parallel computers. Here we concentrate on the strong scaling properties, i.e. the reduction of wall-clock time by running on an increasing number of processors for *the same* simulation setup (i.e. same domain, same number of grid points, same time step, ...). The strong scaling property is important to assess how large a machine must be to tackle a given problem (by the way, strong scaling is a bit easier to investigate than weak scaling with different setups for different processor numbers). We have investigated only CPU based machines, more precise the experiments for both COSMO and ICON have been run on the Cray XC40 (Broadwell) of DWD (i.e. neither GPU based computers nor vector computers have been used).

It is important to mention a difference in the parallelization strategy: COSMO uses only distributed memory parallelization based on the MPI library, In contrast, ICON uses both distributed memory (with MPI) and shared memory parallelization (using openMP).

Fig. 25 shows the strong scaling behavior of COSMO for a COSMO-D2 setup: a simulation over 27 h covering the area of Germany and parts of the surrounding countries. The experiment was carried out with COSMO version 5.4d.4 from 29 May 2017. The strong scaling behavior of the dynamical core (green line) and the physical parameterizations (light blue line) is almost perfect (i.e. linear decrease of wall-cock time) up to about 1000 processors and is still satisfactory at least up to about 10000 processors. The bad scaling of the 'additional computations' is mostly due to the RTTOV library (remark: U. Schättler could cure this problem later on, so that the scaling of these computations now is also quite good). Both the input as also the output don't scale at all: wall-clock times even slightly increase with increasing number of processors.

Fig. 26 shows the analogous strong scaling behavior of ICON for an ICON-D2 setup: it is quite similar to the COSMO-D2 setup, it also runs over 27h and covers roughly the same domain (the output on the regular lat-lon grid is exactly the same horizontally, however the triangle grid covers a slightly larger area). The experiment was carried out with an ICON version from May 2017. As for COSMO, the scaling for the dynamical core and the parameterizations is perfect for up to about 1000 processors. Note that the absolute wall-clock time for the sum of dynamics and physics calculations is smaller than for COSMO. The scaling becomes worse for higher numbers of processors, which is mainly caused by the input of boundary data. Remark: this problem could be largely improved in the meanwhile, in particular by reducing latency by collecting all levels before communication. Moreover, it is worth to mention that ICON allows to optimize the use of the cache by the choice of the so-called `nproma` parameter, i.e. to adapt the length of data blocks to the size of the cache. However, in these tests the value of `nproma` was not changed.

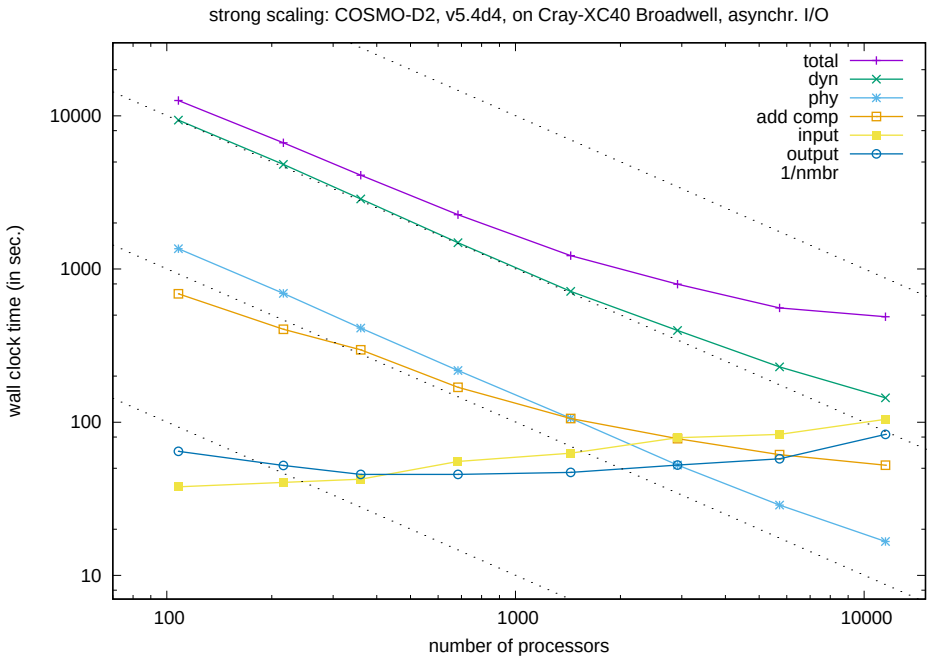

Figure 25: Strong scaling test for COSMO with a COSMO-D2 setup.

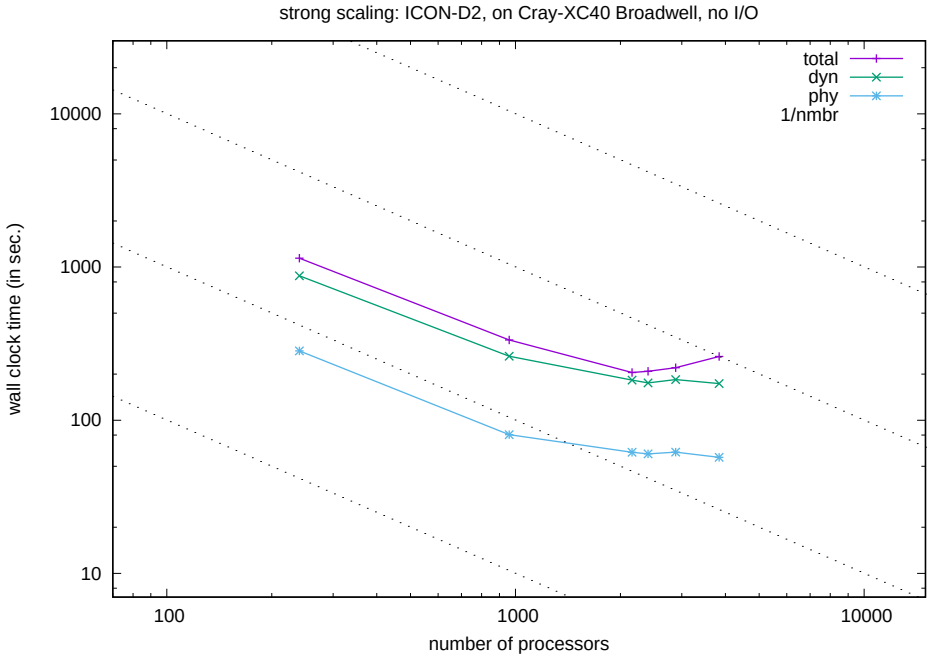

Figure 26: Strong scaling test for ICON with an ICON-D2 setup.

Table 2: List of requirements to the ICON model from climate modelers at DWD.

Issues	Status (around 2017)
Read in LBC Data from frame grid for ICON-LAM does not work yet with NCDF files.	Daniel Reinert and Günther Zängl were already informed.
After restarting, ICON still read the LBC data from the first month.	Already solved in new version.
ICON creates itself a symbolic link to the restart file.	This does not hurt. But just does not look nice and not necessary for us because we have different directories to store data and run the model. One can create the link by a run script and link to wherever
Need to decide a standard input data that iconremap can treat. All GCM data should be transformed to this format.	Task for CLM community.
Soil must be deep enough ($>$ 12 m) that the temperature at the bottom is constant throughout the year (should be the case in Terra).	Will be checked in our long simulation.
Less frequently updated SST.	(addendum: higher frequent updates are now implemented)

5 Application for special purposes (Climate, environmental appl.)

One task in the project was to identify possible obstacles for the use of ICON for other limited-area applications besides pure NWP. First, these are all kind of environmental simulations for several sort of pollutants like pollen, volcanic ash, and radioactive substances. Furthermore, the transport of aerosol or mineral dust in particular for the estimation of the mitigation of solar irradiation for renewable power generation is of interest. In the meanwhile the ART module is well established, so that the applicability of ICON for these purposes is out of question.

Another large application is regional climate simulation. During the project, mainly technical problems have been reported by the climate modelers listed in table 2 (reported by Christian Steger and Trang Van Pham (DWD)). These were mainly assessed as of minor priority, have already been solved in the meanwhile or probably can be solved with relatively low effort. In any case, no basic obstacle could be named for the application of ICON in this field.

6 Conclusions

To assess the ability of the dynamical core of ICON to be applicable for limited-area modeling and to possibly replace the COSMO model, a series of idealized test cases have been performed for both models. These test cases in particular are designed for small scale applications. It may be summarized that ICON delivers in most cases solutions that have similar or even slightly better quality (compared either to analytic solutions or at least to established reference solutions) as COSMO. The only exception is the Straka test case, where ICON delivers a slightly weaker solution; a fact that should be inspected further.

One main strength of ICON is its tolerance of much steeper mountains than COSMO without an additional orography smoothing. Furthermore, it is exactly mass-conserving both for the dry dynamical core and also for the tracers.

The scaling experiments show that ICON runs well on current parallel computers (at least CPU based ones) and its parallelization strategy and implementation is well suited for future massively parallel computers. In practical applications the wall-cock time of ICON is smaller than of COSMO. Remark: more recent results show also an efficient behavior of ICON on vector computers (here in particular on NEC SX Aurora). A GPU port, mainly done at MeteoSwiss, CSCS (Swiss National Supercomputing Centre) and at the DKRZ is widely advanced, too. This efficiency advantage of ICON towards COSMO should also be seen as an indicator, beyond this pure comparison of two particular models, that the split-explicit approach might be less superior to a pure 'single time step' approach than expected.

To summarize, from the viewpoint of the dynamical core, there is no visible obstacle for the replacement of the COSMO model by the ICON model.

References

Baldauf, M., 2008: A linear solution for flow over mountains and its comparison with the COSMO model. *COSMO-Newsletter*, **9**, 19–24, http://www.cosmo-model.org/content/model/documentation/newsLetters/.

Baldauf, M., 2010: Linear stability analysis of Runge-Kutta based partial time-splitting schemes for the Euler equations. *Mon. Wea. Rev.*, **138**, 4475–4496.

Baldauf, M., 2013: A new fast-waves solver for the Runge-Kutta dynamical core. Tech. Rep. 21, Consortium for Small-Scale Modelling (COSMO), 46 pp., http://www.cosmo-model.org/content/model/documentation/techReports/default.htm. doi:10.5676/DWD_pub/nwv/cosmo-tr_21.

Baldauf, M., 2019: Local time stepping for a mass-consistent and time-split advection scheme. *Quart. J. Roy. Met. Soc.*, **145**, 337–346.

Baldauf, M. and S. Brdar, 2013: An analytic solution for linear gravity waves in a channel as a test for numerical models using the non-hydrostatic, compressible Euler equations. *Quart. J. Royal Met. Soc.*, **139**, 1977–1989.

Baldauf, M., A. Seifert, J. Förstner, D. Majewski, M. Raschendorfer, and T. Reinhardt, 2011: Operational Convective-Scale Numerical Weather Prediction with the COSMO Model: Description and Sensitivities. *Monthly Weather Review*, **139**, 3887–3905.

Blahak, U., 2015: Simulating idealized cases with the COSMO-model. *COSMO*.

Bott, A., 1989: A Positive Definite Advection Scheme Obtained by Nonlinear Renormalization of the Advective Fluxes. *Mon. Wea. Rev.*, **117 (5)**, 1006–1015.

Doms, G. and M. Baldauf, 2018: *A Description of the Nonhydrostatic Regional COSMO-Model, Part I: Dynamics and Numerics, v5.05*. Offenbach, Germany, Deutscher Wetterdienst, doi:10.5676/DWD_pub/nwv/cosmo-doc_5.05_I.

Förstner, J., M. Baldauf, and A. Seifert, 2006: Courant Number Independent Advection of the Moisture Quantities for the LMK. *COSMO-Newsletter*, **6**, 51–64, http://www.cosmo-model.org/content/model/documentation/newsLetters/.

Klemp, J. B., J. Dudhia, and A. D. Hassiotis, 2008: An Upper Gravity-Wave Absorbing Layer for NWP Applications. *Mon. Wea. Rev.*, **136**, 3987–4004.

Kurowski, M., D. Wojcik, M. Ziemianski, B. Rosa, and Z. Piotrowski, 2016: Convection-Permitting Regional Weather Modeling with COSMO-EULAG: Compressible and Anelastic Solutions for a Typical Westerly Flow over the Alps. *Mon. Wea. Rev.*, **144**, 1961–1982.

Miura, H., 2007: An Upwind-Biased Conservative Advection Scheme for Spherical Hexagonal-Pentagonal Grids. *Mon. Wea. Rev.*, **135**, 4038–4044.

Schär, C., D. Leuenberger, O. Fuhrer, D. Lüthi, and C. Girard, 2002: A New Terrain-Following Vertical Coordinate Formulation for Atmospheric Prediction Models. *Mon. Wea. Rev.*, **130 (10)**, 2459–2480.

Skamarock, W. C. and J. B. Klemp, 1992: The stability of Time-Split Numerical methods for the Hydrostatic and the Nonhydrostatic Elastic Equations. *Mon. Wea. Rev.*, **120**, 2109–2127.

Skamarock, W. C. and J. B. Klemp, 1994: Efficiency and accuracy of the Klemp-Wilhelmson Time-Splitting scheme. *Mon. Wea. Rev.*, **122**, 2623–2630.

Smith, R. B., 1980: Linear theory of stratified hydrostatic flow past an isolated mountain. *Tellus*, **32**, 348–364.

Straka, J. M., R. B. Wilhelmson, L. J. Wicker, J. R. Anderson, and K. K. Droegemeier, 1993: Numerical solutions of a non-linear density current: a benchmark solution and comparisons. *Int. J. Num. Meth. Fluids*, **17**, 1–22.

Theis, S. and M. Baldauf, 2019: Validation in weather forecasting. *Computer Simulation Validation. Simulation Foundations, Methods and Applications*, C. Beisbart and N. J. Saam, Eds., Springer, Cham, Simulation Foundations, Methods and Applications, 711–736, doi:10.1007/978-3-319-70766-2_29, online ISBN: 978-3-319-70766-2, Print ISBN: 978-3-319-70765-5.

Weisman, M. L. and J. B. Klemp, 1982: The Dependence of Numerically Simulated Convective Storms on Vertical Wind Shear and Buoyancy. *Monthly Weather Review*, **110 (6)**, 504–520.

Wicker, L. J. and W. C. Skamarock, 2002: Time Splitting Methods for Elastic Models using Forward Time Schemes. *Mon. Wea. Rev.*, **130**, 2088–2097.

Zängl, G., 2012: Extending the Numerical Stability Limit of Terrain-Following Coordinate Models over Steep Slopes. *Mon. Wea. Rev.*, **140 (11)**, 3722–3733.

Zängl, G., L. Ganthner, G. Hartjenstein, and H. Noppel, 2004: Numerical errors above steep topography: A model intercomparison. *MetZ*, **13 (2)**, 69–76.

Zängl, G., D. Reinert, P. Ripodas, and M. Baldauf, 2015: The ICON (ICOsahedral Non-hydrostatic) modelling framework of DWD and MPI-M: Description of the non-hydrostatic dynamical core. *Quart. J. Royal Met. Soc.*, **141**, 563–579.

Ziemiański, M. Z., D. K. Wójcik, B. Rosa, and Z. P. Piotrowski, 2021: Compressible EULAG dynamical core in COSMO: convective-scale Alpine weather forecasts. *Mon. Wea. Rev.*, doi:10.1175/MWR-D-20-0317.1.

List of COSMO Newsletters and Technical Reports

(available for download from the COSMO Website: www.cosmo-model.org)

COSMO Newsletters

No. 1: February 2001.

No. 2: February 2002.

No. 3: February 2003.

No. 4: February 2004.

No. 5: April 2005.

No. 6: July 2006.

No. 7: April 2008; Proceedings from the 8th COSMO General Meeting in Bucharest, 2006.

No. 8: September 2008; Proceedings from the 9th COSMO General Meeting in Athens, 2007.

No. 9: December 2008.

No. 10: March 2010.

No. 11: April 2011.

No. 12: April 2012.

No. 13: April 2013.

No. 14: April 2014.

No. 15: July 2015.

No. 16: July 2016.

No. 17: July 2017.

No. 18: November 2018.

No. 19: October 2019.

No. 20: December 2020.

COSMO Technical Reports

No. 1: Dmitrii Mironov and Matthias Raschendorfer (2001):
Evaluation of Empirical Parameters of the New LM Surface-Layer Parameterization Scheme. Results from Numerical Experiments Including the Soil Moisture Analysis.
DOI: 10.5676/DWD_pub/nwv/cosmo-tr_1

No. 2: Reinhold Schrodin and Erdmann Heise (2001):
The Multi-Layer Version of the DWD Soil Model TERRA_LM.
DOI: 10.5676/DWD_pub/nwv/cosmo-tr_2

No. 3: Günther Doms (2001):
A Scheme for Monotonic Numerical Diffusion in the LM.
DOI: 10.5676/DWD_pub/nwv/cosmo-tr_3

No. 4: Hans-Joachim Herzog, Ursula Schubert, Gerd Vogel, Adelheid Fiedler and Roswitha Kirchner (2002):
LLM ¯ the High-Resolving Nonhydrostatic Simulation Model in the DWD-Project LITFASS. Part I: Modelling Technique and Simulation Method.
DOI: 10.5676/DWD_pub/nwv/cosmo-tr_4

No. 5: Jean-Marie Bettems (2002):
EUCOS Impact Study Using the Limited-Area Non-Hydrostatic NWP Model in Operational Use at MeteoSwiss.
DOI: 10.5676/DWD_pub/nwv/cosmo-tr_5

No. 6: Heinz-Werner Bitzer and Jürgen Steppeler (2004):
Documentation of the Z-Coordinate Dynamical Core of LM.
DOI: 10.5676/DWD_pub/nwv/cosmo-tr_6

No. 7: Hans-Joachim Herzog, Almut Gassmann (2005):
Lorenz- and Charney-Phillips vertical grid experimentation using a compressible nonhydrostatic toy-model relevant to the fast-mode part of the 'Lokal-Modell'.
DOI: 10.5676/DWD_pub/nwv/cosmo-tr_7

No. 8: Chiara Marsigli, Andrea Montani, Tiziana Paccagnella, Davide Sacchetti, André Walser, Marco Arpagaus, Thomas Schumann (2005):
Evaluation of the Performance of the COSMO-LEPS System.
DOI: 10.5676/DWD_pub/nwv/cosmo-tr_8

No. 9: Erdmann Heise, Bodo Ritter, Reinhold Schrodin (2006):
Operational Implementation of the Multilayer Soil Model.
DOI: 10.5676/DWD_pub/nwv/cosmo-tr_9

No. 10: M.D. Tsyrulnikov (2007):
Is the particle filtering approach appropriate for meso-scale data assimilation ?
DOI: 10.5676/DWD_pub/nwv/cosmo-tr_10

No. 11: Dmitrii V. Mironov (2008):
Parameterization of Lakes in Numerical Weather Prediction. Description of a Lake Model.
DOI: 10.5676/DWD_pub/nwv/cosmo-tr_11

No. 12: Adriano Raspanti (2009):
COSMO Priority Project "VERification System Unified Survey" (VERSUS): Final Report.
DOI: 10.5676/DWD_pub/nwv/cosmo-tr_12

No. 13: Chiara Marsigli (2009):
COSMO Priority Project "Short Range Ensemble Prediction System" (SREPS): Final Report.
DOI: 10.5676/DWD_pub/nwv/cosmo-tr_13

No. 14: Michael Baldauf (2009):
COSMO Priority Project "Further Developments of the Runge-Kutta Time Integration Scheme" (RK): Final Report.
DOI: 10.5676/DWD_pub/nwv/cosmo-tr_14

No. 15: Silke Dierer (2009):
COSMO Priority Project "Tackle deficiencies in quantitative precipitation forecast" (QPF): Final Report.
DOI: 10.5676/DWD_pub/nwv/cosmo-tr_15

No. 16: Pierre Eckert (2009):
COSMO Priority Project "INTERP": Final Report.
DOI: 10.5676/DWD_pub/nwv/cosmo-tr_16

No. 17: D. Leuenberger, M. Stoll and A. Roches (2010):
Description of some convective indices implemented in the COSMO model.
DOI: 10.5676/DWD_pub/nwv/cosmo-tr_17

No. 18: Daniel Leuenberger (2010):
Statistical analysis of high-resolution COSMO Ensemble forecasts in view of Data Assimilation.
DOI: 10.5676/DWD_pub/nwv/cosmo-tr_18

No. 19: A. Montani, D. Cesari, C. Marsigli, T. Paccagnella (2010):
Seven years of activity in the field of mesoscale ensemble forecasting by the COSMO–LEPS system: main achievements and open challenges.
DOI: 10.5676/DWD_pub/nwv/cosmo-tr_19

No. 20: A. Roches, O. Fuhrer (2012):
Tracer module in the COSMO model.
DOI: 10.5676/DWD_pub/nwv/cosmo-tr_20

No. 21: Michael Baldauf (2013):
A new fast-waves solver for the Runge-Kutta dynamical core.
DOI: 10.5676/DWD_pub/nwv/cosmo-tr_21

No. 22: C. Marsigli, T. Diomede, A. Montani, T. Paccagnella, P. Louka, F. Gofa, A. Corigliano (2013):
The CONSENS Priority Project.
DOI: 10.5676/DWD_pub/nwv/cosmo-tr_22

No. 23: M. Baldauf, O. Fuhrer, M. J. Kurowski, G. de Morsier, M. Müllner, Z. P. Piotrowski, B. Rosa, P. L. Vitagliano, D. Wójcik, M. Ziemiański (2013):
The COSMO Priority Project 'Conservative Dynamical Core' Final Report.
DOI: 10.5676/DWD_pub/nwv/cosmo-tr_23

No. 24: A. K. Miltenberger, A. Roches, S. Pfahl, H. Wernli (2014):
Online Trajectory Module in COSMO: a short user guide.
DOI: 10.5676/DWD_pub/nwv/cosmo-tr_24

No. 25: P. Khain, I. Carmona, A. Voudouri, E. Avgoustoglou, J.-M. Bettems, F. Grazzini (2015):
The Proof of the Parameters Calibration Method: CALMO Progress Report.
DOI: 10.5676/DWD_pub/nwv/cosmo-tr_25

No. 26: D. Mironov, E. Machulskaya, B. Szintai, M. Raschendorfer, V. Perov, M. Chumakov, E. Avgoustoglou (2015):
The COSMO Priority Project 'UTCS' Final Report.
DOI: 10.5676/DWD_pub/nwv/cosmo-tr_26

No. 27: J-M. Bettems (2015):
The COSMO Priority Project 'COLOBOC': Final Report.
DOI: 10.5676/DWD_pub/nwv/cosmo-tr_27

No. 28: Ulrich Blahak (2016):
RADAR_MIE_LM and RADAR_MIELIB - Calculation of Radar Reflectivity from Model Output.
DOI: 10.5676/DWD_pub/nwv/cosmo-tr_28

No. 29: M. Tsyrulnikov and D. Gayfulin (2016):
A Stochastic Pattern Generator for ensemble applications.
DOI: 10.5676/DWD_pub/nwv/cosmo-tr_29

No. 30: D. Mironov and E. Machulskaya (2017):
A Turbulence Kinetic Energy – Scalar Variance Turbulence Parameterization Scheme.
DOI: 10.5676/DWD_pub/nwv/cosmo-tr_30

No. 31: P. Khain, I. Carmona, A. Voudouri, E. Avgoustoglou, J.-M. Bettems, F. Grazzini, P. Kaufmann (2017):
CALMO - Progress Report.
DOI: 10.5676/DWD_pub/nwv/cosmo-tr_31

No. 32: A. Voudouri, P. Khain, I. Carmona, E. Avgoustoglou, J.M. Bettems, F. Grazzini, O. Bellprat, P. Kaufmann and E. Bucchignani (2017):
Calibration of COSMO Model, Priority Project CALMO Final report.
DOI: 10.5676/DWD_pub/nwv/cosmo-tr_32

No. 33: N. Vela (2017):
VAST 2.0 - User Manual.
DOI: 10.5676/DWD_pub/nwv/cosmo-tr_33

No. 34: C. Marsigli, D. Alferov, M. Arpagaus, E. Astakhova, R. Bonanno, G. Duniec, C. Gebhardt, W. Interewicz, N. Loglisci, A. Mazur, V. Maurer, A. Montani, A. Walser (2018):
COsmo Towards Ensembles at the Km-scale IN Our countries" (COTEKINO), Priority Project final report.
DOI: 10.5676/DWD_pub/nwv/cosmo-tr_34

No. 35: G. Rivin, I. Rozinkina, E. Astakhova, A. Montani, D. Alferov, M. Arpagaus, D. Blinov, A. Bundel, M. Chumakov, P. Eckert, A. Euripides, J. Förstner, J. Helmert, E. Kazakova, A. Kirsanov, V. Kopeikin, E. Kukanova, D. Majewski, C. Marsigli, G. de Morsier, A. Muravev, T. Paccagnella, U. Schättler, C. Schraff, M. Shatunova, A. Shcherbakov, P. Steiner, M. Zaichenko (2018):
The COSMO Priority Project CORSO Final Report.
DOI: 10.5676/DWD_pub/nwv/cosmo-tr_35

No. 36: A. Raspanti, A. Celozzi, A. Troisi, A. Vocino, R. Bove, F. Batignani (2018):
The COSMO Priority Project VERSUS2 Final Report.
DOI: 10.5676/DWD_pub/nwv/cosmo-tr_36

No. 37: A. Bundel, F. Gofa, D. Alferov, E. Astakhova, P. Baumann, D. Boucouvala, U. Damrath, P. Eckert, A. Kirsanov, X. Lapillonne, J. Linkowska, C. Marsigli, A. Montani, A. Muraviev, E. Oberto, M.S. Tesini, N. Vela, A. Wyszogrodzki, M. Zaichenko, A. Walser (2019):
The COSMO Priority Project INSPECT Final Report.
DOI: 10.5676/DWD_pub/nwv/cosmo-tr_37

No. 38: G. Rivin, I. Rozinkina, E. Astakhova, A. Montani, J-M. Bettems, D. Alferov, D. Blinov, P. Eckert, A. Euripides, J. Helmert, M.Shatunova (2019):
The COSMO Priority Project CORSO-A Final Report.
DOI: 10.5676/DWD_pub/nwv/cosmo-tr_38

No. 39: C. Marsigli, D. Alferov, E. Astakhova, G. Duniec, D. Gayfulin, C. Gebhardt, W. Interewicz, N. Loglisci, F. Marcucci, A. Mazur, A. Montani, M. Tsyrulnikov, A. Walser (2019):
Studying perturbations for the representation of modeling uncertainties in Ensemble development (SPRED Priority Project): Final Report.
DOI: 10.5676/DWD_pub/nwv/cosmo-tr_39

No. 40: E. Bucchignani, P. Mercogliano, V. Garbero, M. Milelli, M. Varentsov, I. Rozinkina, G. Rivin, D. Blinov, A. Kirsanov, H. Wouters, J.-P. Schulz, U. Schättler (2019):
Analysis and Evaluation of TERRA_URB Scheme: PT AEVUS Final Report.
DOI: 10.5676/DWD_pub/nwv/cosmo-tr_40

No. 41: X. Lapillonne, O. Fuhrer (2020):
Performance On Massively Parallel Architectures (POMPA): Final report.
DOI: 10.5676/DWD_pub/nwv/cosmo-tr_41

No. 42: E. Avgoustoglou, A. Voudouri, I Carmona, E. Bucchignani, Y. Levy, J. -M. Bettems (2020):
A methodology towards the hierarchy of COSMO parameter calibration tests via the domain sensitivity over the Mediterranean area.
DOI: 10.5676/DWD_pub/nwv/cosmo-tr_42

No. 43: H. Muskatel, U. Blahak, P. Khain, A. Shtivelman, M. Raschendorfer, M. Kohler, D. Rieger, O. Fuhrer, X. Lapillonne, G. Rivin, N. Chubarova, M. Shatunova, A. Poliukhov, A. Kirsanov, T. Andreadis, S. Gruber (2021):
The COSMO Priority Project $T^2(RC)^2$: Testing and Tuning of Revised Cloud Radiation Coupling, Final Report
DOI: 10.5676/DWD_pub/nwv/cosmo-tr_43

COSMO Technical Reports

Issues of the COSMO Technical Reports series are published by the *COnsortium for Small-scale MOdelling* at non-regular intervals. COSMO is a European group for numerical weather prediction with participating meteorological services from Germany (DWD, AWGeophys), Greece (HNMS), Italy (USAM, ARPA-SIMC, ARPA Piemonte), Switzerland (MeteoSwiss), Poland (IMGW), Romania (NMA) and Russia (RHM). The general goal is to develop, improve and maintain a non-hydrostatic limited area modelling system to be used for both operational and research applications by the members of COSMO. This system is initially based on the COSMO-Model (previously known as LM) of DWD with its corresponding data assimilation system.

The Technical Reports are intended

- for scientific contributions and a documentation of research activities,
- to present and discuss results obtained from the model system,
- to present and discuss verification results and interpretation methods,
- for a documentation of technical changes to the model system,
- to give an overview of new components of the model system.

The purpose of these reports is to communicate results, changes and progress related to the LM model system relatively fast within the COSMO consortium, and also to inform other NWP groups on our current research activities. In this way the discussion on a specific topic can be stimulated at an early stage. In order to publish a report very soon after the completion of the manuscript, we have decided to omit a thorough reviewing procedure and only a rough check is done by the editors and a third reviewer. We apologize for typographical and other errors or inconsistencies which may still be present.

At present, the Technical Reports are available for download from the COSMO web site (www.cosmo-model.org). If required, the member meteorological centres can produce hard-copies by their own for distribution within their service. All members of the consortium will be informed about new issues by email.

For any comments and questions, please contact the editor:

Massimo Milelli
Massimo.Milelli@arpa.piemonte.it